

# Wingbeat kinematics and motor control of yaw turns in Anna's hummingbirds (*Calypte anna*)

Douglas L. Altshuler<sup>1,2,\*</sup>, Elsa M. Quicazán-Rubio<sup>1,†</sup>, Paolo S. Segre<sup>1,2</sup>, and Kevin M. Middleton<sup>3</sup>

<sup>1</sup>Department of Biology, University of California, Riverside, CA 92521, USA,

<sup>2</sup>Department of Zoology, University of British Columbia, Vancouver, BC V6T 1Z4, Canada

<sup>3</sup>Department of Pathology and Anatomical Sciences, University of Missouri, Columbia, MO 65212, USA.

†Present address: Experimental Zoology Group, Wageningen University, 6709 PG Wageningen, The Netherlands

\*Author for correspondence (doug@zoology.ubc.ca)

Keywords: biomechanics, electromyography, flight, hummingbird, maneuvering, neuromuscular control.

## SUMMARY

The biomechanical and neuromuscular mechanisms used by different animals to generate turns in flight are highly variable. Body size and body plan exert some influence, e.g., birds typically roll their body to orient forces generated by the wings whereas insects are capable of turning via left-right wingbeat asymmetries. Turns are also relatively brief and have low repeatability with almost every wingbeat serving a different function throughout the change in heading. Here we present an analysis of Anna's hummingbirds (*Calypte anna*) as they fed continuously from an artificial feeder revolving around the outside of the animal. This setup allowed for examination of sustained changes in yaw without requiring any corresponding changes in pitch, roll, or body position. Hummingbirds sustained yaw turns by expanding the wing stroke amplitude of the outer wing during the downstroke and by altering the deviation of the wingtip path during both downstroke and upstroke. The latter led to a shift in the inner-outer stroke plane angle during the upstroke and shifts in the elevation of the stroke plane and in the deviation of the wingtip path during both strokes. These features are generally more similar to how insects, as opposed to birds, turn. However, time series analysis also revealed considerable stroke-to-stroke variation. Changes in the stroke amplitude and the wingtip velocity were highly cross-correlated as were changes in the stroke deviation and the elevation of the stroke plane. As was the case for wingbeat kinematics, electromyogram recordings from pectoral and wing muscles were highly variable, but no correlations were found between these two features of motor control. The high variability of both kinematic and muscle activation features indicates a high level of wingbeat-to-wingbeat adjustments during sustained yaw. The activation timing of the muscles was more repeatable than the activation intensity, which suggests that the former may be constrained by harmonic motion and that the latter may play a large role in kinematic adjustments. Comparing the revolution frequency of the feeder to measurements of free flight yaws reveals that feeder tracking, even at one revolution every two seconds, is well below the maximum yaw capacity of the hummingbirds.

## Introduction

Flying animals have the ability to alter velocity and orientation about three axial and three torsional degrees of freedom with varying degrees of independence. This ability is generally termed maneuverability (Dudley, 2000), but this definition does not provide a specific metric that can be compared across individuals or among taxa. Studies with flying birds and bats have sometimes used a specific definition of maneuverability as the smallest radius for which a given animal can make a turn (Pennycuick, 1975). This value is invariant for hovering insects and hummingbirds, which can turn in place. The turning performance of many taxa across a broad range of body sizes has been examined, including insects (Fry et al., 2003; Ristoph et al., 2009; Springthorpe et al., 2012; Hedrick et al., 2009), fishes (Weihs, 1972; Webb, 1983), birds (Warrick et al., 1988; Warrick and Dial, 1998; Hedenström and Rosén, 2001; Hedrick and Biewener, 2007; Hedrick et al., 2007; Ros et al., 2011), bats (Norberg and Rayner, 1987; Iriarte-Díaz and Swartz, 2008), carnivorous mammals (Eilam, 1994), and humans (Carrier et al., 2001; Lee et al., 2001). These studies have revealed a diversity of biomechanical mechanisms for turning, even within clades of flying animals such as birds or insects. One source of this variation is that turns can be composed of different magnitudes and phases of body pitch, roll, and yaw. Thus, even for a specific definition of maneuverability in flight, it is unknown which, if any, kinematic features are necessarily conserved among animal species or across body sizes.

Hovering insects and hummingbirds provide an opportunity for comparing maneuvering performance because these animals can all turn in place about the yaw axis with little or no change about roll and pitch axes and no change in horizontal or vertical position. Experiments with tethered fruit flies (*Drosophila melanogaster*; Götz, 1968) and locusts (*Locusta migratoria*; Dawson et al., 1997) have demonstrated that during attempted turns, the inner wing (the inner forewing for the locusts) sweeps through a smaller arc, i.e., has lower stroke amplitude, compared to the outer wings. Tethered locusts also exhibit a pronounced asymmetry in the average elevation of the fore wings with the inner wing being more depressed (Dawson et al., 1997). When generating yaw turns in free flight, the outer wing of *D. melanogaster* has a wider stroke amplitude and a more horizontal stroke, i.e., a shallower stroke plane angle, which also causes an increase in the angle of attack of the outer wing (Fry et al., 2003). A universal mechanism for terminating yaw turns in freely flying insects and hummingbirds is the use of symmetrical wingbeat kinematics because the difference in velocity experienced by each wing

79 during the turn is sufficient to damp the yaw torque (Hedrick et al., 2009). The kinematic  
80 mechanisms that hummingbirds use to generate yaw turns have not been investigated previously  
81 although more complicated escape maneuvers have been described (Christopher James Clark,  
82 2010).

83 Any difference between left and right wingbeat kinematics must be reflected in the  
84 activation features of at least one bilateral pair of muscles. Numerous recordings from the basalar  
85 muscles of tethered insects have revealed that the activation phase and number of spikes are  
86 associated with changes in wing deviation and stroke amplitude (Dawson et al., 1997; Tu and  
87 Dickinson, 1996; Lehmann and Götz, 1996). When larger groups of muscles are recorded  
88 simultaneously, subsets have been found to act synergistically (Heide, 1975). For example, two  
89 of the basalar muscles of tethered blowflies (*Calliphora vicina*) are associated with wing  
90 downstroke deviation, and interactions among basalar and pterale III muscles influence the  
91 stroke amplitude (Balint and Dickinson, 2001). Recordings from freely flying *Convolvulus*  
92 Hawkmoths (*Agrius convolvuli*; Ando et al., 2002) further demonstrate associations between the  
93 timing on direct muscles in the insect thorax and the stroke amplitude and deviation (Wang et al.,  
94 2008). Timing differences in the main power muscles, the dorsal longitudinal and dorsal ventral  
95 muscles, of the Tobacco Hawkmoth (*Manduca sexta*) influences the overall yaw velocity of the  
96 body in free flight, but do so by acting upon the inertial velocity that is extended from the  
97 previous stroke (Springthorpe et al., 2012).

98 The activation patterns of avian muscles are more difficult to interpret because the large  
99 number of motoneurons innervating each muscle leads to considerable variation in timing  
100 (temporal recruitment patterns) and intensity (spatial recruitment patterns). Hedrick and  
101 Biewener (Hedrick and Biewener, 2007) recorded from two pectoral muscles (pectoralis major  
102 and supracoracoideus) and two wing muscles (biceps brachii and extensor metacarpi radialis) as  
103 Rose-breasted cockatoos (*Eolophus roseicapillus*) navigated a 90° turn. They observed left-right  
104 activation asymmetries in all of the muscles, but none of these patterns were associated with  
105 among-wingbeat changes in body kinematics. Hummingbirds can hover like many insects and,  
106 during this behavior, the pectoralis major has a relatively simple activation pattern composed of  
107 only 1-3 spikes (Hagiwara et al., 1968). Experiments in low-density air, during load lifting, and  
108 in a wind tunnel demonstrate an association between the maximum EMG spike amplitude from  
109 this muscle and the wingstroke amplitude (Altshuler et al., 2010; Tobalske et al., 2010). The

hummingbird therefore presents an opportunity to examine neuromuscular and kinematic mechanisms of turning in birds that can be directly compared to the extensive literature on insect flight control.

For the present study, we sought to address three questions: 1) What are the wingbeat kinematic and neuromuscular features used by hummingbirds to generate sustained yaw turns? 2) How repeatable are these features? 3) What are the temporal associations between muscle activation patterns and wingbeat kinematics? To address these questions, we trained hummingbirds to track a feeder that revolved around the outside of the animal thereby eliciting a pure yaw turn, without any change in roll, pitch, horizontal or vertical position. The hummingbirds tracked the feeder for several seconds, amounting to as many as a hundred or more wingbeats. During these steady-state maneuvers, we recorded the wingbeat kinematics using high-speed cameras and made electromyogram recordings (EMGs) from the pectoralis major, pronator profundus, and pronator superficialis muscles. Associations among kinematic and electrophysiological variables are examined using several statistical approaches including time series analysis.

## MATERIALS AND METHODS

### Animals

Between May and September of 2009, we captured four adult male Anna's hummingbirds (*Calypte anna*) at the University of California, Riverside campus, using portable drop-door traps and Hall traps (Russell and Russell, 2001). The hummingbirds were housed individually in cages measuring 0.93m x 0.62m x 0.62m and fed *ad libitum* with a solution of 13% artificial nectar (Nektar-Plus, Nekton GmbH, Germany) and 5% sucrose. The light cycle in the vivarium was 12:12 with lights on from 7 a.m. to 7 p.m. Prior to experiments, the animals were brought to the laboratory for three to four days of training and acclimation to the flight chamber. All the procedures were conducted under permits from the United States Fish and Wildlife Service and the California Department of Fish and Game, and approved by the Institutional Animal Care and Use Committee at the University of California, Riverside.

### Experimental setup and training

The flight chamber (Fig. 1A) was 0.61m high, 0.58m deep, and 0.51m wide and contained a wooden perch in one corner and an artificial feeder made out of a 1mL syringe that was mounted at the end of a J-shaped aluminum arm. The long arm was connected to a stepper motor (MDrive 23 Plus, Schneider Electric Motion, USA) placed in the center of the cage roof. The distance between the mouth of the feeder and the axis of rotation of the motor was adjusted slightly, if needed, for each bird such that they could feed from the revolving syringe while maintaining their center of gravity in the axis of feeder rotation, thereby executing a pure yaw turn.

An individual hummingbird was initially moved from the vivarium, placed in the experimental chamber, and trained for the experiment. They first learned to feed on command from the stationary feeder by covering it for 20 minutes in between feeding bouts. As soon as a bird terminated a feeding bout by flying away, the feeder was once again covered. Within one to three hours, each bird learned to approach the feeder as soon as access was allowed and then feed for bouts longer than 5 seconds. Thereafter, the bird learned to feed while the feeder was rotated at a slow frequency of 7.5 revolutions per minute (r.p.m.). We maintained this frequency until the hummingbird consistently followed the feeder for two seconds and then increased the revolution frequencies to 15, 25 and finally 30 r.p.m., which was the frequency used for all experiments with the turning feeder. The birds were trained equally on both clockwise and counterclockwise directions at all training frequencies. Each hummingbird typically required three days of training, four hours per day before they could follow the feeder consistently at 30 r.p.m. (0.5 Hz).

### **Surgery and experimental procedures**

Hummingbirds were anesthetized with isoflurane during the surgical procedure to implant the electromyography (EMG) and ground wires. Induction concentrations were 2.5%, but the isoflurane concentration was brought to 1.8% as quickly as possible once the animals reached a surgical plane. Oxygen flow rates were maintained at 500cc/min. Each animal had four recording electrodes implanted into muscles, two on each side. Our intention was to target the pectoralis major (PM) and the pronator superficialis (PS) on both the left and right sides. The PM was targeted because it powers the downstroke and its activity varies in response to mechanical demands (Hagiwara et al., 1968; Altshuler et al., 2010; Tobalske et al., 2010). The PS was

targeted because it is one of the larger superficial muscles in the hummingbird wing (Welch Jr. and Altshuler, 2009). It is nonetheless a very small muscle and we inadvertently recorded from two other proximal wing muscles, the pronator profundus (PP) and the flexor digitorum superficialis (FDS) in place of recordings intended from the PS.

The EMG wires were made of 99.99% silver with heavy polyimide (HML) insulation (California Fine Wire, USA). The vendor fabricated electrically isolated wire pairs ("bifilar") made of either 0.0508 mm (0.002") or 0.0762 mm (0.003") diameter wires. We used the 0.0508 mm electrodes with the proximal wing muscles (FDS, PP, and PS), and the 0.0762 mm electrodes with the pectoralis major (PM). A single 0.1016 mm (0.004") silver wire, also insulated with HML, served as the ground electrode. We removed the last 0.5mm of insulation from the end of each wire, and offset the ends of the paired wires by 0.5 mm.

To secure the electrodes around the muscle fibers, we fed the end of the wire or wire pair into the tip of a hypodermic needle and then bent back the wire to form a hook. We then inserted the recording electrodes into the muscles and the ground electrode subcutaneously on the back above the vertebral column using the needle. We removed the needle and left the wires in place by holding it with forceps as the needle was removed. The electrodes were secured with 6-0 sutures to the skin of the hummingbird over the site of insertion and additionally secured the full set of lead wires with suture through the intervertebral fascia.

Following recovery from the initial surgery, hummingbirds were released in the flight chamber. Three different flight behaviors were recorded: stationary hovering, clockwise turning, and counterclockwise turning. All recordings with the revolving feeder were made at 30 r.p.m. Two trial recordings of each flight behavior were made for each bird with one exception: only one trial was made for bird 4 during hovering. The trials and behaviors were varied in temporal sequence. A trial was considered successful if the bird fed from the feeder for at least 0.5 seconds. Trials were separated by 20 minutes and all the trials for each bird were recorded in a single day. Following data collection, each bird was briefly anesthetized with isoflurane and the electrodes were removed taking care to prevent damage to muscle fibers. The body mass was recorded on a digital scale and the wings on both sides of the bird were photographed in an outstretched position against white paper with a reference scale. Measurements of wing length, wing area, aspect ratio, and the non-dimensional moments of wing area were calculated using custom analysis software in Matlab (Mathworks Inc., USA).



## Electromyography

EMG signals from the electrodes were amplified x1000 using a multi-channel extracellular amplifier (model 1700, A-M Systems, USA), with the low- and high-frequency cutoffs of the online filters set at 0.1 Hz and 10 kHz, respectively. The amplifier output was acquired at 10,000 samples per second (0.1 ms resolution) with an analog-to-digital acquisition board (Digidata 1440, Molecular Devices, USA). The electrophysiology data were synchronized with the high-speed cameras (1 ms resolution) by recording the camera trigger pulse with the acquisition system.

The EMG signals were filtered offline using zero-phase, fourth-order high-pass Butterworth filters with cut-off frequencies set at between 3-12 times the wingbeat frequency. The wing strokes were defined by the furthest angular extents within the stroke plane to determine the relative timing of excitation events. All EMG analyses were performed separately for the left and right wings because the angular extreme sometimes occurred at different times.

The muscle activation timing and intensity were examined using different representations depending upon the muscle (Table 1). The PM is unusual in having a relatively small number of discrete excitation waveforms, and the spike amplitudes are correlated with wingbeat kinematics and flight speeds (Hagiwara et al., 1968; Altshuler et al., 2010; Tobalske et al., 2010). We accordingly used the occurrence of the first spike ( $\hat{t}$ ) as the measure of activation timing relative to the wingbeat, and the normalized maximum spike amplitude ( $\hat{E}_{\max}$ ) as the measure of activation intensity. The proximal wing muscles have more typical vertebrate activation patterns in that the burst duration is longer and a greater number of waveforms are present. We accordingly used the average spike occurrence ( $\bar{t}$ ) relative to the wingbeat for activation timing, and the normalized, rectified area of the waveform ( $\hat{E}_{\text{area}}$ ) as the measure of activation intensity. The timing and activation variables were calculated over a wingbeat cycle beginning and ending at the upstroke-downstroke transition (pronation) for the PM and PS. The wingbeat cycle for the PP began and ended at the downstroke-upstroke transition (supination). Because the PP and PS have biphasic activation patterns, we analyzed the first and second bursts independently. We recorded the FDS from only one side of one animal, which was insufficient to include its excitation features in the analysis. We normalized both measures of EMG intensity by first calculating the log of each variable per wingbeat cycle and then confirming that the maximum



value was not an outlier. All of the intensity measures for a single electrode were then divided by the maximum value for that electrode.

### Kinematic digitization

High-speed images of each hummingbird flying in the cage were recorded in three views by two cameras. One camera (Troubleshooter, Fastec Imaging, USA) recorded at 640 x 480 pixel resolution through a mirror placed at an angle of 45° under the chamber, providing the bottom view of the hummingbird. A second camera (Miro 4, Vision Research, USA) recorded the front view and a side view. The side view was filmed through a second mirror placed outside the left wall of the chamber and tilted at an angle of 45°. This camera recorded both perspectives using an aspect ratio and resolution of 800 x 600 pixels. Both cameras filmed at 1000 frames s<sup>-1</sup> with a shutter speed of 1/5000 sec. The image sequences in both cameras terminated with a common end trigger thereby synchronizing the videos.

The three camera views were calibrated using the direct linear transformation (DLT) technique with a 14-point calibration frame and DLTdv3 software (Hedrick, 2008). Six points were digitized on each hummingbird: left wing tip, right wing tip, right shoulder, left shoulder, top of the head and the tip of the middle tail feather. Every third frame in each video was digitized, and the resulting data were fit with a cubic spline to extrapolate the points in the remaining frames. These splined 2D points were then checked and refined frame-by-frame within DLTdv3. After the 2D points were refined, the 3D real-world body points were filtered with zero-phase, fourth-order low-pass Butterworth filters. The filter cutoff frequencies ranged between 1.5 and 5 times the wingbeat frequency, with generally lower cut-off frequencies for the head position and higher cutoff frequencies for the tail, wing shoulder, and wingtip positions.

The images were sampled at 1000 frames per second, which translated to ~25 frames per wingbeat or ~25 time points per wing and body point. To improve the estimate of the maximum and minimum excursions and their phasing with respect to EMGs, the filtered kinematic data were upsampled to 10,000 frames per second and fit with a cubic spline using the interpolate package from the Scientific Tools for Python (SciPy) module. This procedure increased precision in the calculation of wing angles, stroke duration and muscle activation phase relative to wing motion. The pronation time for each wing was defined as the time of the minimum excursion in the stroke plane whereas the supination time was defined by the maximum

excursion. The pronation and supination times were used to calculate the wing stroke durations and for the relative timings of the muscle activation features.

### Frame of reference and coordinate system

We compared the kinematics across wingbeats using two frames of reference, both defined in part by the position of the wings at the start and end of each downstroke and upstroke (Fig. 1B). We used wing stroke-centered frames of reference because the tail exhibited high frequency oscillations (Altshuler et al., 2009) and the body position varied within and among trials. One frame of reference was constrained by gravity and other was aligned with the stroke plane.

In the gravitational frame of reference (Fig. 2A), the Z-axis was set parallel to gravity, thereby defining an X-Y plane parallel to the ground. Each wing stroke was rotated about the Z-axis by defining the X-axis as a line located in between the left and right wingtip paths projected into the X-Y plane. The midpoints between the wingtips at the upstroke-downstroke transition and downstroke-upstroke transition were used to calculate the wingtip path dividing line. Thus, the frame of reference rotated for each stroke, and kinematic parameters were calculated for down- and up-strokes separately. The yaw angle  $\Psi$  was defined as the angular rotation between strokes (Fig. 1B), and the number of values per trial was therefore twice the number of wingbeats. Within the gravitational frame of reference, positive Z was towards the sky and the bird faced the positive direction of the X-axis. This frame of reference allowed us to maintain the aerodynamic relevance to gravity but still compare the paths of each individual wing strokes.

The stroke plane-centered frame of reference (Fig. 2B) differed from the gravitational frame of reference in two respects: 1) The Z'-axis was orthogonal to the stroke plane; 2) The stroke planes, and therefore the frames of reference, were calculated separately for the left and right wings. This transformation allowed for comparison of the deviations from the stroke plane between the left and right wings, across wingbeats, and among animals.

### Kinematic variables

We defined 10 kinematic variables, which were calculated separately for each down- and up- stroke (Table 1). Yaw angle was described above for the frames of reference. Six variables were calculated in the gravitational frame of reference. The wingtip speed  $U_{\text{tip}}$  was calculated by

dividing the distance traveled through the three dimensions by the duration of the stroke. The body axis was defined as a line through the head and tail, and its orientation with respect to the horizontal plane and the bird's orientation provided two body angles. The lateral body angle  $\chi_{GR, XZ}$  was calculated in the X-Z plane and the frontal body angle  $\chi_{GR, YZ}$  was calculated in the Y-Z plane.

Two wing angles were calculated for each time step with respect to gravity. The instantaneous position angle  $\phi_{GR}$  describes the angle between the shoulder to wingtip vector and the Y-axis, projected into the X-Y plane (Fig. 2A). The values are constrained between  $-90^\circ$  (directly behind the bird) and  $+90^\circ$  (directly in front of the bird). The instantaneous elevation angle  $\theta_{GR}$  describes the angle between the shoulder to wingtip vector and its projection in the X-Y plane. Its values are constrained between  $-90^\circ$  (directly below the bird) and  $+90^\circ$  (directly above the bird). The average of the elevation angle for each stroke  $\bar{\theta}_{GR}$  provides the position of the stroke plane relative to the shoulder.

The stroke plane was determined using reduced major axis (RMA) regression of the wingtip positions in the X-Z plane for each wing in each stroke. The stroke plane angle  $\beta$  is the angle between the slope of the RMA regression and the horizontal plane (Fig. 2B). Negative values indicate that the beginning of the stroke is at a higher elevation than the end of the stroke. The wing stroke amplitude  $\Phi_{SP}$  is the angle from the rearward most position of the wingtip to the shoulder to the forward most position of the wingtip, projected into the stroke plane. The elevation amplitude  $\Theta_{SP}$  is the sum of the maximum and minimum angles, each defined as an angle between the shoulder to wingtip vector and its projection into the stroke plane. The frame of reference transformations and the calculations of the kinematic variables were made using custom software written in Python (Python Software Foundation, 2012).

### Statistical analysis

Sequences of wingbeat kinematics and muscle activations represent time series data. We used four statistical approaches to analyze how these variables changed across flight modes. All statistical analyses were implemented in R (R Development Core Team, 2012).

The variation in the kinematic and EMG variables by flight mode was compared using the intra-class correlation coefficient (ICC), which is the most common measure of repeatability.

The specific method was analysis of variance (ANOVA)-based (Lessells and Boag, 1987; Whitlock and Schluter, 2009). The EMG values were considered separately for the left and right sides. The kinematic values were assessed for left-right differences for the down- and up-strokes separately. The two trials of each flight mode were combined for ICC analysis.

To examine overall changes in mean values of kinematic and electromyographic parameters, we employed a mixed-model ANOVA with flight mode (hover, clockwise, and counter-clockwise) as the fixed effect and bird as a random effect. For kinematic variables, downstroke and upstroke were separated. The ANOVA approach led to a massive reduction in the data set, utilizing a mean value for each measure for each bird per flight mode. We chose to use a single mean instead of a more complicated mixed-model ANOVA (e.g., trial nested within bird), because of low variance within measures per bird-flight mode combination. For models with significant overall ANOVAs ( $\alpha < 0.05$ ), a post-hoc analysis was employed to test for significant differences between clockwise and hovering and between counter-clockwise and hovering using general linear hypothesis tests corrected for multiple comparisons (Hothorn et al., 2008).

The third approach was to use time series analysis to consider how the relationships between kinematic and electromyography measures changed through time. We first calculated the autocorrelation (AC), which is the cross-correlation of each individual measure with a 32-time point (i.e., 16 downstroke-upstroke pairs), time-lagged version of itself (Venables and Ripley, 2002). Using a similar approach, we then examined cross-correlations (CC) among pairwise combinations of all variables (kinematic vs. kinematic and kinematic vs. electromyographic) for the same 16 wingbeats. Because the sequences of wingbeats were too short for standard time series detrending procedures, which are used to remove non-stationarity from time series data (Cowpertwait and Metcalfe, 2009), we implemented a method based on linear regression. We first determined the ordinary least squares regression slope of each observation of each variable versus time (wing stroke period 1-32). We then used the two-dimensional rotation matrix to rotate the data so that the new slope was zero.

We assessed significance of AC analyses by aggregating the proportion of each measure with at least one non-zero lag value whose correlation fell outside a 95% confidence interval for autocorrelation. We used only non-zero lags because the correlation at lag = 0 is 1 by definition and, thus, is always significant. Significance among CC analyses was assessed via

randomization. For each set of variables (kinematic vs. kinematic and kinematic vs. electromyographic), we generated a null distribution for each variable for each of lags = -2, -1, 0, 1, and 2. This range of lags corresponds to a period including synchronous correlation (lag = 0) as well as correlations of  $\pm 1/2$  and  $\pm 1$  wingbeat. An analytical  $P$ -value for each variable-lag combination was determined as median of the proportion of times that the observed CC exceeded the randomized CC. Because checking over 1,000 distributions for normality was impractical, we chose to use the median, which is a better estimator of central tendency for skewed distributions and converges on the mean for normally distributed samples. This method produced more conservative results than assessing the likelihood of significance based on the percentage of significant CC analyses for each variable-lag combination.

The fourth approach, principal components analysis (PCA) was carried out to confirm the results of the ANOVA and cross-correlation analyses among kinematic variables only. Due to the incomplete nature of the electromyographic data, these data could not be included in the PCA analysis. All variables were scaled to unit variance prior to the analysis.

## RESULTS

The body mass and wing morphology of the four *C. anna* used in experiments are given in table 2. Separate measurements were made on the left and right wings and paired t-tests were used to determine if the wing morphology variables differed by side. Although there were small asymmetries for each of the wing variables, there was no systematic difference by side (all  $P > 0.45$ ).

Representative electromyograms are provided in figure 3. These raw recordings were made with the online analog filters wide open and have not been post processed. The signals come from different individuals during hovering flight. The pectoralis major (PM) and the three wing muscles [flexor digitorum superficialis (FDS), pronator profundus (PP), and pronator superficialis (PS)] come from the birds in the present study. A verified recording from the supracoracoideus (SC) of a different individual adult male *C. anna* is also presented for comparison. Other than electrode placement, the SC recording was made with identical methods to the PM recordings.

The PM becomes active midway through the upstroke and likely generates muscle force at stroke transition and during the subsequent downstroke. The PS and FDS become active at the

downstroke-upstroke transition and presumably generate force during the latter half of the upstroke, possibly continuing through stroke transition. The FDS was not recorded with sufficient sample size for analysis but it is included here because the position of the electrode that recorded this trace was confirmed post mortem. The SC becomes active midway through the downstroke and likely generates muscle force at stroke transition and during the subsequent upstroke. The PP becomes active during the upstroke-downstroke transition and probably generates force during the latter half of the downstroke, continuing through stroke transition.

The revolving feeder had a constant rotation of 30 r.p.m., but the hummingbirds did not track the feeder with constant angular velocity and instead varied the yaw angles by stroke (Fig. 1C). The maximum angular changes in left (counter-clockwise,  $-7.9^\circ$ ) and right (clockwise,  $11.4^\circ$ ) yaw angle were recorded during downstrokes. The birds exhibited small changes in yaw during hovering (blue traces) at a stationary feeder.

The average wingbeat frequencies and left-right differences in stroke amplitude are given for the four individuals in table 3. Among individuals, wingbeat frequencies varied as much as 4 Hz within a flight mode, but within individuals this value was less than 1 Hz across the three flight modes. The differences in left-right stroke amplitude were similar between up- and downstrokes for each individual during hovering flight. The values for clockwise flight were always more positive for the downstroke, whereas the counter-clockwise values were more positive for the upstroke. Thus, the outer-inner difference in stroke amplitude was consistently higher on the downstroke compared to the upstroke.

The instantaneous wing position angles in the gravitational frame of reference were sinusoidal and highly repeatable for both wings across wingbeats for all three treatments (Fig. 4). The instantaneous elevation angles were also similar between left and right wings, and across wingbeats during hover feeding. However, these traces were much more variable during clockwise and counterclockwise feeder tracking. In these cases, the left and right wings exhibited divergent patterns that also varied considerably across wingbeats.

### Intra-class Correlation

The intra-class correlation (ICC) or repeatability values for the timing and intensity features of the PM, PP, and PS are provided in table 4. The negative values arise when there is greater variability within than among individuals. However, it has been suggested that this

situation is unlikely to occur in nature and that negative values represent statistical noise around what is effectively zero repeatability (Nakagawa and Schielzeth, 2010). Across all muscles and flight modes, the average ICC for the timing features ( $\bar{x} = 0.59$ ) is higher than for the intensity features ( $\bar{x} = 0.27$ ). During hovering flight, the repeatability of the timing features is higher or nearly so compared to the other flight modes. For the intensity features, the repeatability values for the PM were generally higher or nearly so compared the other two muscles.

The ICC values for the kinematic variables spanned a wide range (Table 5). The most consistently low values were for the yaw angles during both strokes, further demonstrating that the hummingbird tracked the revolving feeder with high variation across strokes. The stroke amplitudes and the wingtip velocities exhibited relatively high repeatability for both strokes across all three maneuvers. This was also the case for the average elevation angle but the ICC values for the elevation amplitude were relatively low. The body angles and stroke plane angles exhibited a broader range in ICC values.

### Mixed-Model ANOVA

The mixed-model ANOVAs revealed broad patterns of differences in mean kinematic measures across flight maneuvers (Tables 6,7) with no significant differences in electromyographic measures (all  $P > 0.2$ ). Significant differences were found among flight modes in yaw angle ( $\Psi$ ), average elevation angle ( $\bar{\theta}_{GR}$ ), and elevation amplitude ( $\theta_{\square\square}$ ) for both upstroke and downstroke, stroke plane angle ( $\beta$ ) during upstroke, and stroke amplitude ( $\phi_{SP}$ ) during downstroke. Based on post-hoc tests comparing clockwise and counter-clockwise maneuvers with hovering, clockwise maneuvers are more different from hovering than are counter-clockwise maneuvers. The kinematic variable with strongest differences between hovering and yaw maneuvers is the average elevation angle ( $\bar{\theta}_{GR}$ ). The complete data set for this variable during the downstroke as well as several other kinematic and electromyographic variables are provided in figure 5. In addition to wingbeat- and stroke-specific values, these plots contain the mean values by bird and maneuver, which are the inputs to the mixed-model ANOVAs. This approach clearly eliminates time-varying patterns of potential interest for understanding flight control.

### Time series analysis



A large number of variables had at least one non-zero lag correlation that fell outside a 95% confidence interval (online supplementary Table S1). The muscle activation features were autocorrelated in 43% of all trials. Kinematic variables were autocorrelated in 71% of the trials, and some variables, such as body angles, average elevation angles, elevation amplitudes and stroke plane angles were autocorrelated in almost every trial. Two general patterns of autocorrelation are present: (1) sinusoidal autocorrelation at low frequencies, which characterize changes in body angles and (2) alternating autocorrelation, corresponding to differences between upstrokes and downstrokes, which characterize stroke plane angle, elevation angle, elevation amplitude, and wingtip speed (Fig. 6).

There are a large number of cross comparisons among kinematic and electromyographic variables. The cross-correlation analysis between kinematics and EMGs is composed of 800 variable combinations with a sample size of 8,640 for all four individuals. Comparisons within kinematics are composed of 280 variable combinations with a sample size of 6,440. When analyzed without correcting for multiple comparisons, many of the kinematic and electromyographic combinations appear to show significant cross-correlation, e.g., the average time of the first burst of the PS with kinematic measures at multiple lags (Online Supplementary Figure S1). However, subsequent randomization analysis demonstrated that significant cross-correlation is highly probable for randomly ordered data, resulting in no significant *P*-values across all 800 comparisons ( $P > 0.06$ ; Online Supplementary Figure S2). Patterns of cross-correlation among kinematic measures are widespread, both considering percentage significant (Online Supplementary Figure S3) and *P*-value via randomization (Fig. 7). Significant cross-correlations at lags  $\pm\frac{1}{2}$  and  $\pm 1$  wingbeat are widespread among kinematic measures. The strongest ( $P < 0.005$ ) and most consistent (present on both sides) cross-correlations were between average elevation angle and elevation amplitude, and between stroke amplitude and wingtip speed, all at zero lag.

### Principal Components Analysis

Principal components analysis showed kinematic measures to co-vary largely independently of one another (Online supplementary materials: Figure S3; Table S2). Only yaw angle ( $\Psi$ ) and frontal body angle ( $\chi_{GR, XZ}$ ) loaded similarly on the first and second PCs. All other

variables loaded differently from each other on the first two PCs. In contrast to most PCAs, the proportion of variance accounted for by the first two PCs was just over half.

## DISCUSSION

### Overall Kinematic Changes

Hummingbirds sustain yaw turns using two distinct kinematic mechanisms: 1) extending the stroke amplitude of the outer wing during the downstroke, and 2) substantially altering the deviation path of both wings during both strokes. For the first mechanism, it is important to note that our frames of reference are set by the extreme positions of the wing strokes. The feeder revolved at an angular rate of  $\sim 4.5^\circ$  per wingbeat or  $\sim 2.25^\circ$  per wing stroke given the near constant wingbeat frequency. If a hummingbird tracked the feeder at the same rate while using a constant stroke amplitude with respect to its body, its expected left-right stroke amplitude difference is  $4.5^\circ$  per stroke or  $9.0^\circ$  per wingbeat. During clockwise turns, the average left-right stroke amplitude during the downstroke was  $3.75^\circ$ , and during counterclockwise turns, the average value was  $-8.49^\circ$ . During hovering, the average downstroke value was  $-4.02^\circ$ , which was significantly different from the values exhibited during turning (Table 7). Because the measured values fall close to, or within, the range of the expected values during turns it is not known the extent to which the asymmetry in stroke amplitudes was a cause or a consequence of yaw torque. The asymmetries are nonetheless a relevant feature given that variation in wing stroke amplitude is one of the primary mechanisms that hummingbirds use to control aerodynamic power (Chai and Dudley, 1995; Altshuler et al., 2010; Tobalske et al., 2007, 2010).

Asymmetries in the deviation path of the wings leads to the outer wing in a more elevated position and with a higher absolute deviation in the U-shaped trajectory during both strokes as well as an increase in the stroke plane angle during the upstroke. These overall changes are apparent by comparing the time course of wing angle values in the gravitational frame of reference (Fig. 8) and by plotting the wing tip traces relative to body models in the three planes of the gravitation frame of reference (Fig. 9). Hummingbirds exhibit these stroke specific changes in wingbeat kinematics while holding similar average body positions during stationary hovering and yaw turns to the left and right. Hummingbird yaw kinematics share similarities with measurements of attempted turns in tethered insects and real turns in freely flying insects,

but also differ in key elements. Comparing hummingbird yaw turns to *Drosophila* free flight saccades (Fry et al., 2003) reveals that both animals expand the stroke amplitude of the outer wing, but the fruit flies reduce its deviation and stroke plane angle whereas the hummingbirds increase elevation amplitude ( $\theta_{SP}$ ) during both strokes, and stroke plane angle ( $\beta$ ) during the upstroke. The hummingbird yaw turns also share asymmetry in inner and outer stroke amplitudes with the *Drosophila* “Sashay maneuvers” (Ristroph et al., 2009), which have a strong yaw component, but again differ with respect to deviation and stroke plane angle between the inner and outer wings.

A key turning-related kinematic feature identified from insect studies is the orientation or pitch angle of the wing in a body- or stroke-centered frame of reference, and the related angle of attack in a velocity frame of reference. Difference between inner and outer wings in the absolute rotation angles as well as the timing of rotation have been reported for tethered insects during attempted turns with varying degrees of freedom (Baker, 1979; Zarnack, 1988; Waldmann and Zarnack, 1988; Schwenne and Zarnack, 1987; Thüring, 1986; Dawson et al., 1997) and for the free flight turns of *Drosophila* (Fry et al., 2003; Ristroph et al., 2009). Our analysis did not include this feature, but there are at least two ways in which it can be very important to generating force asymmetries. Advances in the timing of wing rotation can contribute to enhanced lift (Dickinson et al., 1999) as has been demonstrated for hovering honey bees (Altshuler et al., 2005). However, even if rotational lift does not apply, left-right differences in rotation timing will influence the aerodynamic forces produced during the wing translation.

Other than hummingbirds, the birds that have been studied use fundamentally different biomechanical mechanisms to change heading during flight. Ros et al. (Ros et al., 2011) recently demonstrated that turning in flying pigeons is controlled not by altering wingbeat kinematics but by reorienting the body to direct aerodynamic forces. They also pointed out that other birds (Warrick and Dial, 1998; Hedrick and Biewener, 2007) and bats (Aldridge, 1986, 1987; Iriarte-Díaz and Swartz, 2008) roll during aerial turns, which suggests that many volant vertebrates may be limited in their ability to orient aerodynamic forces off the body axis. Our results are not directly comparable to all features of the Ros et al. (Ros et al., 2011) study because we used stroke-averaged kinematics for comparisons, but the differences in stroke amplitude and deviation combined with the lack of difference in mean body position angles among flight modes indicates that hummingbirds are able to redirect forces relative to their bodies. Although Anna’s

hummingbirds are much smaller than the turning birds and bats that have been studied so far, there is considerable overlap in size between the larger hummingbird species and the smaller bird and bat species. Measurements from these animals would elucidate if the differences observed so far derive from body size or from differences in body plan between hovering and non-hovering animals.

### Muscle Activations

The activation bursts of the hummingbird pectoral muscles, the pectoralis major and supracoracoideus, contain fewer spikes and are more advanced in relative wingbeat timing compared to the pigeon and other avian taxa (Tobalske et al., 2010). The activations of avian wing muscles have received relatively little attention with the exception of some extensive recordings by Dial with pigeons and starlings (Dial et al., 1991; Dial, 1992a, 1992b). Comparing the pronator superficialis between the hummingbird and the pigeon (Dial, 1992a) reveals that the relative duration is similar between the two taxa but that the relative timing is advanced in the hummingbird. To the best of our knowledge no comparable recordings are available for the pronator profundus and flexor digitorum superficialis from other birds during flight, and it remains to be tested if advanced timing is a feature of all hummingbird wing muscles.

The timing of muscle activations of the pectoralis major, pronator profundus, and pronator superficialis was more repeatable than the intensity of the activations during hovering and yaw turns (Table 4). There were no activation features consistently associated with experimental treatments, and none of the activation features were cross-correlated with kinematic variables across time. The activation timing of the PM and its antagonist, the supracoracoideus, sets the wingbeat frequency. The kinematic correlates of the activation timings of the PP and PS have not yet been described but these may be constrained by the need to rotate the wing during stroke transition. The spike amplitude of the PM has also been demonstrated to vary consistently with the stroke amplitude as hummingbirds adjust to low air density air, lift weights (Altshuler et al., 2010) or fly at faster speeds in a wind tunnel (Tobalske et al., 2010). The role of variation in the spike amplitude of the PM as well as the intensity of the PP and PS during yaw turns is not clear at the present time. It may be that the wing control is best understood in terms of synergies among a larger group of muscles (d'Avella and Tresch, 2001; d'Avella et al., 2003), which has

also been suggested to explain a lack of strong associations between individual muscle activation patterns and wingbeat kinematics in maneuvering cockatiels (Hedrick and Biewener, 2007).

### Time Series Analysis

Taking mean values of the kinematic and electromyographic variables and comparing these across treatments revealed significant differences in the former but not the latter. However, focusing on average values can be misleading because the animals exhibited considerable stroke-to-stroke differences, even during hovering flight. The yaw angle values did not trend monotonically during clockwise and counter-clockwise feeder tracking, meaning for example that during a clockwise turn, or either of the other two treatments, the hummingbird might be yawing left, right, or holding steady during any one particular wing stroke (Fig. 1). Two distinct patterns of autocorrelation were observed, sinusoidal fluctuations and oscillations between subsequent down- and up- strokes. Further analysis of the sinusoidal patterns is limited due to sample size. Sixteen wingbeats strikes a balance between digitizing effort for a number of birds/trials and the likelihood of finding a significant temporally distant pattern. It would be highly informative to conduct a spectral analysis of wingbeat-to-wingbeat variation when more automated digitizing techniques and longer time series become available. This will also reveal if the apparent dextral bias in some birds (Fig. 10) is an innate property or an artifact of low sample size.

Many of the kinematic features varied through time in a coordinated fashion (Fig. 7). The two strongest associations included some of the kinematic features that are also most strongly associated with feeder tracking. Wing stroke amplitude and wingtip speed were cross-correlated indicating the importance of velocity asymmetries because the aerodynamic forces are proportional to the square of the wing velocity. The wing elevation and the elevation amplitude were also cross-correlated indicating the importance of orientating the net force in the desired direction of movement.

We are not aware of other comparable data sets that include EMG timing and intensity measures and wingbeat kinematics on freely flying animals during sustained turns. The published measurements of wingbeat kinematics from insects and birds span several wingbeats over which the maneuver is continuously changing. In the current study, hummingbirds sustained maneuvering behavior over many wingbeats although stroke-to-stroke variation was readily

apparent. Variability of both kinematics and muscle activations have received considerable attention in the human biomechanics literature (recently reviewed in Stergiou and Decker, 2011). A key idea is that variation in motor features can indicate flexibility and control of complex motor behavior. For example, as humans repetitively practice some types of novel task, limb kinematics become less variable whereas EMG recordings, in contrast, can become more variable (Darling and Cooke, 1987). When increasing the speed of certain types of limb movements, the variability of both kinematics and electromyographic features tends to decrease (Carlton et al., 1985; Li et al., 2005). If similar principles apply to avian flight control then the variation in muscle intensity features may be exerting stronger influence compared to muscle timing features on stroke-to-stroke variation in wingbeat kinematics.

### Comparisons with free flight yaw turns

The purpose of the present study was to examine the neuromuscular and kinematic mechanisms that hummingbird employ to sustain yaw turns. The experimental approach constrained the hummingbirds to track a revolving feeder without any requirement for changes in pitch, roll, or vertical or lateral body position. As has been demonstrated for free flying insects during turns, hummingbirds execute yaw through expansion of the outer stroke amplitude and shifts in the stroke plane and deviation path of both wings. However, we observed considerable wingbeat-to-wingbeat variation in kinematic and electromyographic variables, and we did not detect any consistent relationship between kinematics and muscle activations. Taken together, these results suggest that hummingbirds make fine adjustments over very short time scales to track a feeder at the angular velocities under consideration here.

To place this experimental-induced behavior in the context of more natural flight behaviors, we finally consider the distribution of yaw velocities recorded from four different *Calypte anna* males during solitary, feeding and competitive flights in a large flight chamber (1.5 x 1.5 x 3.0 m). The position and orientation of these birds was tracked using the *Flydra* system originally developed for fruit flies (Straw et al., 2011). The cameras recorded at 200 frames per second and the data set come from 44 hours of recordings. The most significant distinction between the free flight yaw velocities presented in figure 10 and the yaw velocities from the feeder tracking experiment is that the former are determined by position differences over 5 ms whereas the latter are stroke averages over a slightly longer period of ~13 ms.

Hummingbird yaw turns from the revolving feeder experiment closely matched how they turned in free flight. The feeder was revolved by the motor at 0.5 revolutions per second because this was the angular velocity at which all four birds sustained feeder tracking. This value was similar to the median free flight yaw velocities of 0.46 and 0.48 revolutions per second for the left and right turns, respectively. The maximum yaw velocities recorded during feeding tracking and free flight were also similar. The strokes with fastest yaw velocities during feeder tracking were 1.85 and 2.43 rev/sec for left and right turns, respectively. The maximum values for free flight yaw velocities are represented by the 97.5% value of the frequency distribution, which was 2.32 rev/sec and 2.33 rev/sec for left and right turns. The close correspondence in velocities indicates that the feeder tracking experiment provided a relevant test of average yaw turns. Nonetheless, it is readily apparent that tracking the revolving feeder at the imposed angular velocities required much lower values in yaw velocity than the hummingbirds are capable of performing in free flight. We conclude by suggesting that the kinematic and muscle activation variability observed during feeder tracking reflects fine motor control adjustments across wingbeats, indicating that the hummingbirds were controlling sub-maximal behavior.



**ACKNOWLEDGEMENTS**

We gratefully acknowledge support from undergraduate research assistants, our colleagues, and funding agencies. Bobby Chi, Anita Lakhani, Aleck von Mueller, and Cristina Soto assisted with digitation of wingbeat kinematics. Robert Donovan, Benny Goller, Carlo Segre, and Ken Welch provided technical advice. Two anonymous reviewers gave very helpful comments on the manuscript. The U.S. National Science Foundation (IOS 0923849 and IOS 0923802) and the Natural Sciences and Engineering Research Council of Canada (402667) provided financial support during data collection, analysis, and manuscript composition.

## REFERENCES

- Aldridge, H. D.** (1986). Kinematics and aerodynamics of the greater horseshoe bat, *Rhinolophus ferrumequinum*, in horizontal flight at various flight speeds. *J Exp Biol*, **126**, 479–497.
- Aldridge, H. D.** (1987). Turning flight of bats. *J Exp Biol*, **128**, 419–425.
- Altshuler, D. L., Dickson, W. B., Vance, J. T., Roberts, S. P., and Dickinson, M. H.** (2005). Short-amplitude high-frequency wing strokes determine the aerodynamics of honeybee flight. *Proc Nat Acad Sci USA*, **102**, 18213–18218.
- Altshuler, D. L., Princevac, M., Pan, H., and Lozano, J.** (2009). Wake patterns of the wings and tail of hovering hummingbirds. *Exp Fluids*, **46**, 835–846.
- Altshuler, D. L., Welch, K. C., Cho, B. H., Welch, D. B., Lin, A. F., Dickson, William B., and Dickinson, M. H.** (2010). Neuromuscular control of wingbeat kinematics in Anna's hummingbirds (*Calypte anna*). *J Exp Biol*, **213**, 2507–2514.
- Ando, N., Shimoyama, I., and Kanzaki, R.** (2002). A dual-channel FM transmitter for acquisition of flight muscle activities from the freely flying hawkmoth, *Agrius convolvuli*. *J Neurosci Meth*, **115**, 181–187.
- d' Avella, A., Saltiel, P., and Bizzi, E.** (2003). Combinations of muscle synergies in the construction of a natural motor behavior. *Nat Neurosci*, **6**, 300–308.
- d' Avella, A. and Tresch, M. C.** (2001). Modularity in the motor system: decomposition of muscle patterns as combinations of time-varying synergies. In, *NIPS*, pp. 141–148.
- Baker, P. S.** (1979). The wing movements of flying locusts during steering behaviour. *J Comp Physiol A*, **131**, 49–58.
- Balint, C. N. and Dickinson, M. H.** (2001). The correlation between wing kinematics and steering muscle activity in the blowfly *Calliphora vicina*. *J Exp Biol*, **204**, 4213–4226.
- Carlton, M. J., Robertson, R. N., Carlton, L. G., and Newell, K. M.** (1985). Response timing variability: coherence of kinematic and EMG parameters. *J Mot Behav*, **17**, 301–319.
- Carrier, D. R., Walter, R. M., and Lee, D. V.** (2001). Influence of rotational inertia on turning performance of theropod dinosaurs: clues from humans with increased rotational inertia. *J Exp Biol*, **204**, 3917–3926.
- Chai, P. and Dudley, R.** (1995). Limits to vertebrate locomotor energetics suggested by hummingbirds hovering in heliox. *Nature*, **377**, 722–725.
- Clark, Christopher James** (2010). Effects of tail length on an escape maneuver of the Red-billed Streamertail. *J Ornithol*, **152**, 397–408.

- 691 **Cowpertwait, P. S. P. and Metcalfe, A. V.** (2009). Introductory Time Series with R  
692 Springer, New York.
- 693 **Darling, W. G. and Cooke, W. G.** (1987). Movement related EMGs become more variable  
694 during learning of fast accurate movements. *J Mot Behav*, **19**, 311–331.
- 695 **Dawson, J. W., Dawson-Scully, K., Robert, D., and Robertson, R. M.** (1997). Forewing  
696 asymmetries during auditory avoidance in flying locusts. *J Exp Biol*, **200**, 2323 –  
697 2335.
- 698 **Dial, K. P.** (1992a). Activity patterns of the wing muscles of the pigeon (*Columba livia*)  
699 during different modes of flight. *J Exp Zool*, **262**, 357–373.
- 700 **Dial, K. P.** (1992b). Avian forelimb muscles and nonsteady flight: can birds fly without  
701 using the muscles in their wings? *Auk*, **109**, 874–885.
- 702 **Dial, K. P., Goslow, G. E., and Jenkins, F. A.** (1991). The functional anatomy of the  
703 shoulder in the european starling (*Sturnus vulgaris*). *J Morph*, **207**, 327 – 344.
- 704 **Dickinson, M. H., Lehmann, F.-O., and Sane, S. P.** (1999). Wing rotation and the  
705 aerodynamic basis of insect flight. *Science*, **284**, 1954–1960.
- 706 **Dudley, R.** (2000). The Biomechanics of Insect Flight Princeton University Press, Princeton,  
707 New Jersey.
- 708 **Eilam, D.** (1994). Influence of body morphology on turning behavior in carnivores. *J Mot*  
709 *Behav*, **26**, 3–12.
- 710 **Fry, S. N., Sayaman, R., and Dickinson, M. H.** (2003). The aerodynamics of free-flight  
711 maneuvers in *Drosophila*. *Science*, **300**, 495–498.
- 712 **Götz, K. G.** (1968). Flight control in *Drosophila* by visual perception of motion. *Kybernetik*,  
713 **4**, 199–208.
- 714 **Hagiwara, S., Chichibu, S., and Simpson, N.** (1968). Neuromuscular mechanisms of wing  
715 beat in hummingbirds. *Z Vergl Physiol*, **60**, 209–218.
- 716 **Hedenström, A. and Rosén, M.** (2001). Predator versus prey: on aerial hunting and escape  
717 strategies in birds. *Behav Ecol*, **12**, 150 –156.
- 718 **Hedrick, T. L.** (2008). Software techniques for two- and three-dimensional kinematic  
719 measurements of biological and biomimetic systems. *Bioinspir Biomim*, **3**, 034001.
- 720 **Hedrick, T. L. and Biewener, A. A.** (2007). Low speed maneuvering flight of the rose-  
721 breasted cockatoo (*Eolophus roseicapillus*). I. kinematic and neuromuscular control  
722 of turning. *J Exp Biol*, **210**, 1897–1911.

- 723 **Hedrick, T. L., Cheng, B., and Deng, X.** (2009). Wingbeat time and the scaling of passive  
724 rotational damping in flapping flight. *Science*, **324**, 252–255.
- 725 **Hedrick, T. L., Usherwood, J. R., and Biewener, A. A.** (2007). Low speed maneuvering  
726 flight of the rose-breasted cockatoo (*Eolophus roseicapillus*). II. Inertial and  
727 aerodynamic reorientation. *J Exp Biol*, **210**, 1912–1924.
- 728 **Heide, G.** (1975). Properties of a motor output system involved in the optomotor response  
729 in flies. *Biol Cybern*, **20**, 99–112.
- 730 **Hothorn, T., Bretz, F., and Westfall, P.** (2008). Simultaneous inference in general  
731 parametric models. *Biometrical J*, **50**, 346–363.
- 732 **Iriarte-Díaz, J. and Swartz, S. M.** (2008). Kinematics of slow turn maneuvering in the fruit  
733 bat *Cynopterus brachyotis*. *J Exp Biol*, **211**, 3478–3489.
- 734 **Lee, D. V., Walter, R. M., Deban, S. M., and Carrier, D. R.** (2001). Influence of increased  
735 rotational inertia on the turning performance of humans. *J Exp Biol*, **204**, 3927–  
736 3934.
- 737 **Lehmann, F.-O. and Götz, K. G.** (1996). Activation phase ensures kinematic efficacy in  
738 flight-steering muscles of *Drosophila melanogaster*. *J Comp Physiol A*, **179**, 311–322.
- 739 **Lessells, C. M. and Boag, P. T.** (1987). Unrepeatable repeatabilities: A common mistake.  
740 *Auk*, **104**, 116–121.
- 741 **Li, L., Haddad, J. M., and Hamill, J.** (2005). Stability and variability may respond  
742 differently to changes in walking speed. *Hum Move Sci*, **24**, 257–267.
- 743 **Nakagawa, S. and Schielzeth, H.** (2010). Repeatability for Gaussian and non-Gaussian  
744 data: a practical guide for biologists. *Biological Reviews*, **85**, 935–956.
- 745 **Norberg, U. M. and Rayner, J. M. V.** (1987). Ecological morphology and flight in bats  
746 (Mammalia; Chiroptera): wing adaptations, flight performance, foraging strategy  
747 and echolocation. *Phil Trans Roy Soc Lond B*, **316**, 335–427.
- 748 **Pennycuik, C. J.** (1975). Mechanics of flight. In, Farner, D. S., King, J. R., and Parkes, K. C.  
749 (eds), *Avian Biology*. Academic Press, London, pp. 1–75.
- 750 **Python Software Foundation** (2012). Python.
- 751 **R Development Core Team** (2012). R: A Language and Environment for Statistical  
752 Computing, Version 2.15.0 R Foundation for Statistical Computing, Vienna, Austria.
- 753 **Ristroph, L., Berman, G. J., Bergou, A. J., Wang, Z. J., and Cohen, I.** (2009). Automated  
754 hull reconstruction motion tracking (HRMT) applied to sideways maneuvers of free-  
755 flying insects. *J Exp Biol*, **212**, 1324–1335.

- 756 **Ros, I. G., Bassman, L. C., Badger, M. A., Pierson, A. N., and Biewener, A. A.** (2011).  
 757 Pigeons steer like helicopters and generate down- and upstroke lift during low  
 758 speed turns. *Proc Nat Acad Sci USA*, **108**, 19990–19995.
- 759 **Russell, S. M. and Russell, R. O.** (2001). The North American Banders' Manual for Banding  
 760 Hummingbirds The North American Banding Council, Point Reyes Station, CA.
- 761 **Schwenne, T. and Zarnack, W.** (1987). Movements of the hindwings of *Locusta*  
 762 *migratoria*, measured with miniature coils. *J Comp Physiol A*, **160**, 657–666.
- 763 **Springthorpe, D., Fernández, M. J., and Hedrick, T. L.** (2012). Neuromuscular control of  
 764 free-flight yaw turns in the hawkmoth *Manduca sexta*. *J Exp Biol*, **215**, 1766–1774.
- 765 **Stergiou, N. and Decker, L. M.** (2011). Human movement variability, nonlinear dynamics,  
 766 and pathology: Is there a connection? *Hum Movement Sci*, **30**, 869–888.
- 767 **Straw, A. D., Branson, K., Neumann, T. R., and Dickinson, M. H.** (2011). Multi-camera  
 768 real-time three-dimensional tracking of multiple flying animals. *J Roy Soc Inter*, **8**,  
 769 395–409.
- 770 **Thüring, D. A.** (1986). Variability of motor output during flight steering in locusts. *J Comp*  
 771 *Physiol A*, **158**, 653–664.
- 772 **Tobalske, B. W., Biewener, A. A., Warrick, D. R., Hedrick, T. L., and Powers, D. R.**  
 773 (2010). Effects of flight speed upon muscle activity in hummingbirds. *J Exp Biol*, **213**,  
 774 2515–2523.
- 775 **Tobalske, B. W., Warrick, D. R., Clark, Christopher J., Powers, D. R., Hedrick, T. L.,**  
 776 **Hyder, G. A., and Biewener, A. A.** (2007). Three-dimensional kinematics of  
 777 hummingbird flight. *J Exp Biol*, **210**, 2368–2382.
- 778 **Tu, M. S. and Dickinson, M. H.** (1996). The control of wing kinematics by two steering  
 779 muscles of the blowfly (*Calliphora vicina*). *J Comp Physiol A*, **178**, 813–830.
- 780 **Venables, W. N. and Ripley, B. D.** (2002). Modern Applied Statistics with S. Fourth ed.  
 781 Springer, New York.
- 782 **Waldmann, B. and Zarnack, W.** (1988). Forewing movements and motor activity during  
 783 roll manoeuvres in flying desert locusts. *Biol Cybern*, **59**, 325–335.
- 784 **Wang, H., Ando, N., and Kanzaki, R.** (2008). Active control of free flight manoeuvres in a  
 785 hawkmoth, *Agrius convolvuli*. *J Exp Biol*, **211**, 423–432.
- 786 **Warrick, D. R. and Dial, K. P.** (1998). Kinematic, aerodynamic and anatomical  
 787 mechanisms in the slow, maneuvering flight of pigeons. *J Exp Biol*, **201**, 655–672.
- 788 **Warrick, D. R., Dial, K. P., and Biewener, A. A.** (1988). Asymmetrical force production in  
 789 the maneuvering flight of pigeons. *Auk*, **115**, 916–928.

- 790 **Webb, P. W.** (1983). Speed, acceleration and manoeuvrability of two teleost fishes. *J Exp*  
791 *Biol*, **102**, 115–122.
- 792 **Weihs, D.** (1972). A hydrodynamical analysis of fish turning manoeuvres. *Proc Roy Soc B*,  
793 **182**, 59–72.
- 794 **Welch Jr., K. C. and Altshuler, D. L.** (2009). Fiber type homogeneity of the flight  
795 musculature in small birds. *Comp Biochem Phys B*, **152**, 324–331.
- 796 **Whitlock, M. C. and Schluter, D.** (2009). The Analysis of Biological Data. Roberts and  
797 Company Publishers, Greenwood Village, Colorado, USA.
- 798 **Zarnack, W.** (1988). The effect of forewing depressor activity on wing movement during  
799 locust flight. *Biol Cybern*, **59**, 55–70.
- 800

## FIGURE LEGENDS

**Figure 1.** Hummingbirds performed yaw turns while tracking a revolving feeder in a flight chamber (A). The feeder was mounted to a J-shaped aluminum arm that was itself connected to a stepper motor. The arm was adjusted for each bird so that the bird's center of mass was located at the motor's axis of rotation. The feeder was covered in between feeding trials and the bird was provided with a perch at all times. Electromyograms from up to four muscles were recorded using trailing leads that connected to an extracellular amplifier. The frame of reference was defined in part by the position of the wings for each stroke (B). Downstrokes are indicated in orange with the tail, shoulder, and wingtip positions indicated by a point for each video frame. Upstrokes are indicated with maroon. The angular change in the wingbeat-centered frame of reference between strokes is given by the yaw angle  $\Psi$ . In this example from a counterclockwise turn, the  $\Psi$  values for 29 sequential strokes are depicted in the maroon-orange curve. The indent represents several strokes during which the hummingbird did not vary  $\Psi$ . The  $\Psi$  values for all of the hummingbirds included in the study are provided in a polar diagram (C). Any change along the radius indicates a change in  $\Psi$  for that stroke. The sequences differed with respect the number of wingbeats digitized. Experiments are color coded with blue indicating hovering at the stationary feeder, and green and red indicating feeder revolution in the counterclockwise and clockwise directions, respectively.

**Figure 2.** Within the gravitational frame of reference, the wings elevation angle ( $\theta_{GR}$ ) and stroke position angle ( $\phi_{GR}$ ) were calculated for each image frame (A). The stroke plane frame of reference was shifted by the stroke plane angle ( $\beta$ ), and the elevation amplitude ( $\theta_{SP}$ ) and stroke amplitude ( $\phi_{SP}$ ) were calculated once per stroke (B).

**Figure 3.** Raw electromyogram recordings from five flight muscles in *Calypte anna*. The signals were acquired with the online analog filters wide open and are presented without post processing. Four wing strokes are depicted for each muscle. Downstrokes are indicated by gray bars and upstrokes are in white. The voltage increments of the y-axis



have been scaled for each panel so that each muscle trace spans the same range. The recordings come from different individuals but the time scale is the same for all traces. The recordings of the pectoralis major, pronator superficialis, pronator profundus, and flexor digitorum superficialis come from the present study. A verified recording of the supracoracoideus using identical methods but from a different individual is also included.

**Figure 4.** Representative traces in the gravitational frame of reference. The position angle  $\phi_{GR}$  and elevation angle  $\theta_{GR}$  are presented for 15 wingbeats across three trials, one each of clockwise, hovering, and counterclockwise flight. The left wing is indicated in red and the right wing is indicated in blue. Downstrokes are shaded in gray and upstrokes are in white. Discontinuities between strokes result from shifts in the frame of reference.

**Figure 5.** Representative electromyographic and kinematic variables through time. The data are presented from left to right in order (within each trial) as the individual wingbeats or strokes with trial 1 preceding trial 2. The scale bar represents the length of most of the trials. The colors indicate the four individuals in the study (red = bird 1, blue = bird 2, green = bird 3, purple = bird 4). For the EMG variables (A-D), triangles indicate the muscles of the right wing and crosses indicate the muscles of the left wing. For the kinematic variables (E, F) filled circles representing the left-minus right values. The timing values for the PM (A) and both bursts of the PP (B) are the first spike time ( $\hat{t}$ ) and the average spike time of each burst ( $\bar{t}$ ), respectively. The intensity values for the PM (C) and the first burst of the PP (D) are the normalized maximum spike amplitude ( $\hat{E}_{max}$ ) and the rectified area of the waveform ( $\hat{E}_{area}$ ), respectively. The representative kinematic variables are the difference in the stroke plane angle ( $\beta$ , E) and average elevation angle ( $\bar{\theta}_{GR}$ , F) during downstrokes. All wingbeats (A-D) and downstrokes (E, F) were used for the time series analysis but the mixed model ANOVAs included only the averages by bird and maneuver (large circles with black centers).

**Figure 6.** Representative autocorrelation functions. The change in kinematic variables through time are provided for the lateral body angle (A) and average elevation angle on the right wing (C) during the first hovering trial of bird #2. The downstrokes are indicated in solid black circles and the upstrokes are indicated in white circles. The corresponding autocorrelations are provided on the right (B, D). The autocorrelation lags are defined per stroke. In general, significant autocorrelations for the body angles consisted of sinusoidal time series, and significant autocorrelations for the wing angles consisted of alternative times series for the down- and up- strokes.

**Figure 7.** Matrix of significance for cross-correlations between kinematic variables as determined by generation of null distribution for each variable for each set of lags. The lags are defined as wingbeats with strokes representing steps of  $\frac{1}{2}$ . The color map for probabilities ranges from red (significant for  $P$ 's < 0.05) to blue (non-significant). Cross-correlations among kinematic variables on the left side of the animals are provided in the left columns and cross-correlations among kinematics on the right side are shown in the right columns. Symbols are defined in table 1.

**Figure 8.** Average kinematic traces in the gravitational frame of reference. The mean time course of the position angles  $\phi_{GR}$  and elevation angles  $\theta_{GR}$  are presented twice to allow for comparison across wingbeats. The left wing is indicated in red and the right wing is indicated in blue. Shading corresponds to the standard deviations across all four birds. Downstrokes are shaded in gray and upstrokes are in white. Discontinuities between strokes result from shifts in the frame of reference.

**Figure 9.** Average kinematic traces plotted on the body from the front (top row), side (middle row), and top (bottom row) perspectives. Clockwise turns are depicted in the left column, hovering flight is depicted in the middle column, and counter-clockwise turns are depicted in the right column. The left wing is indicated in red and the right wing is indicated in blue. The mean values for each bird were calculated for all wingbeats in each treatment. The mean values plotted here were calculated across all four birds. Discontinuities between strokes result from shifts in the frame of reference.

**Figure 10.** Distribution of instantaneous yaw velocities recorded from the solitary and paired flights of four male *C. anna*. Values come from free flight recordings of birds during feeding, exploratory, and competitive flights. The data elements are yaw velocities > 0.25 revolutions per second measured from sequential frame pairs filmed at 200 fps in which the birds held a body attitude between 60-80° relative to the horizontal plane and did not exhibit a substantial change in pitch, horizontal, or vertical velocity. Negative x-axis values indicate leftward yaw velocities (red) and positive values indicate rightward yaw velocities (blue). The solid black arrows indicate the angular velocity of the motors used for the feeder tracking experiments and the dashed black arrows represent the maximum left and right yaw velocities recorded during these experiments. The feeder tracking data are not represented in the frequency distribution of the instantaneous yaw velocities.

## ONLINE FIGURES:

**Figure S1.** Matrix showing the proportion of cross-correlations between kinematic and electromyographic variables with  $P$ -values  $< 0.05$  before correcting for multiple comparisons. The lags are defined as wingbeats with strokes representing steps of  $\frac{1}{2}$ . The color map for proportions ranges from red (none of the cross-correlation pairs are significant) to blue (most of the of cross-correlation pairs are significant). The kinematic variables include the average elevation angle ( $\bar{\theta}_{GR}$ ), body angle frontal ( $\chi_{GR, YZ}$ ), body angle lateral ( $\chi_{GR, XZ}$ ), elevation amplitude ( $\phi_{SP}$ ), stroke amplitude ( $\phi_{SP}$ ), stroke plane angle ( $\beta$ ), yaw angle ( $\psi$ ), and wingtip speed ( $U_{tip}$ ). Muscle variables include the occurrence of the first spike ( $t$ ) and the normalized maximum spike amplitude ( $\hat{E}_{max}$ ) of the pectoralis major (PM), and the average spike occurrence ( $\bar{t}$ ) and rectified area of the waveform ( $\hat{E}_{area}$ ) of bursts 1 and 2 of the pronator profundus (PP) and pronator superficialis (PS). Cross-correlations among kinematic variables on the left side of the animals are provided in the left columns and cross-correlations among kinematics on the right side are shown in the right columns.

**Figure S2.** Matrix of significance for cross-correlations between kinematic and electromyographic variables as determined by generation of null distribution for each variable for each set of lags. The color map for probabilities ranges from red (strong trends but non-significant) to blue (non-significant). Symbols and arrangements for the variables are given in table 1 and figure S1.

**Figure S3.** Matrix showing the proportion of cross-correlations between kinematic variables with  $P$ -values  $< 0.05$  before correcting for multiple comparisons. The color map for proportions ranges from red (none of the cross-correlation pairs are significant) to blue (most of the of cross-correlation pairs are significant). Symbols and arrangements for the kinematic variables are given as in table 1 and figure 7.

935 **Figure S4:** Results of principal components analysis of kinematic measures. (A)  
936 Cumulative proportion of variance explained by the eight principal components. In  
937 contrast to most PCA analyses, the cumulative proportion of variance explained  
938 increases almost linearly over the first six PCs. The first two PCs only account for 51%  
939 of the variance. (B) Biplot of PC2 vs. PC1 with arrows showing the loading vectors for  
940 each of the kinematic measures. With the exception of Body Angle Frontal and Yaw  
941 Angle, no two variables load together consistently on PC1 and PC2.

Figure 1

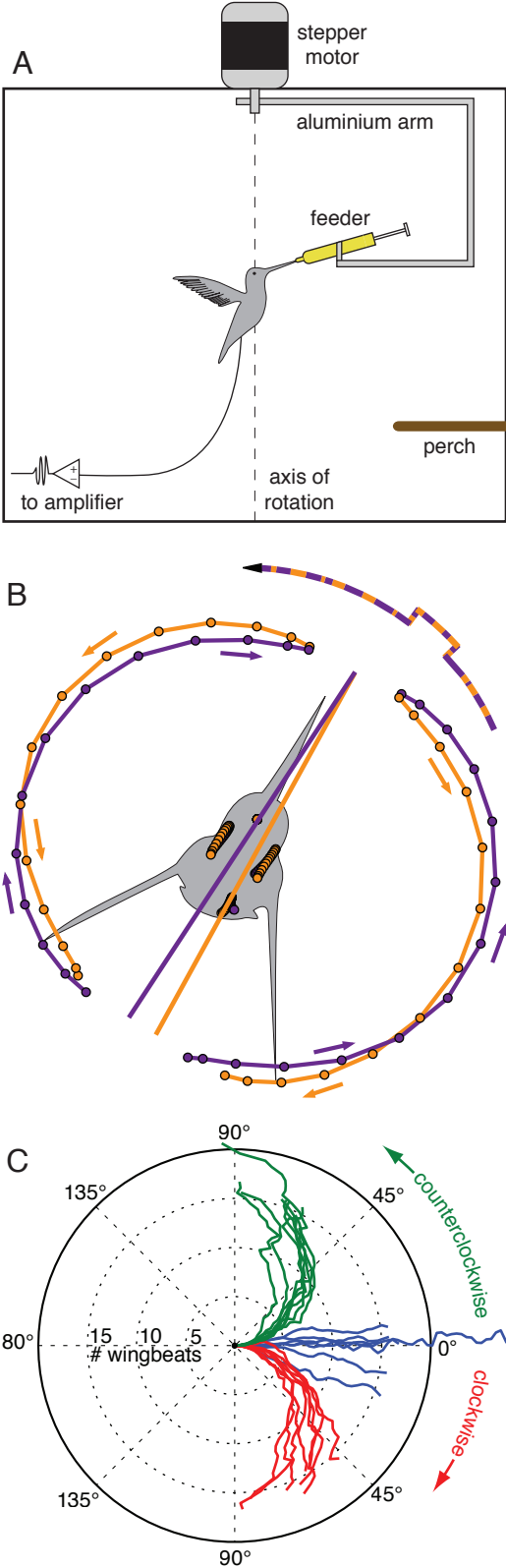


Figure 2

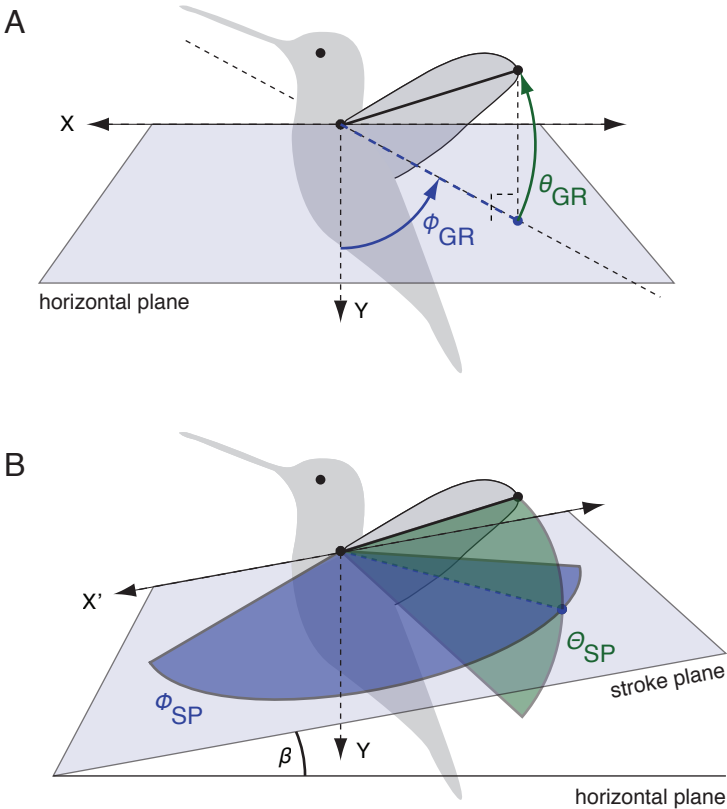




Figure 3

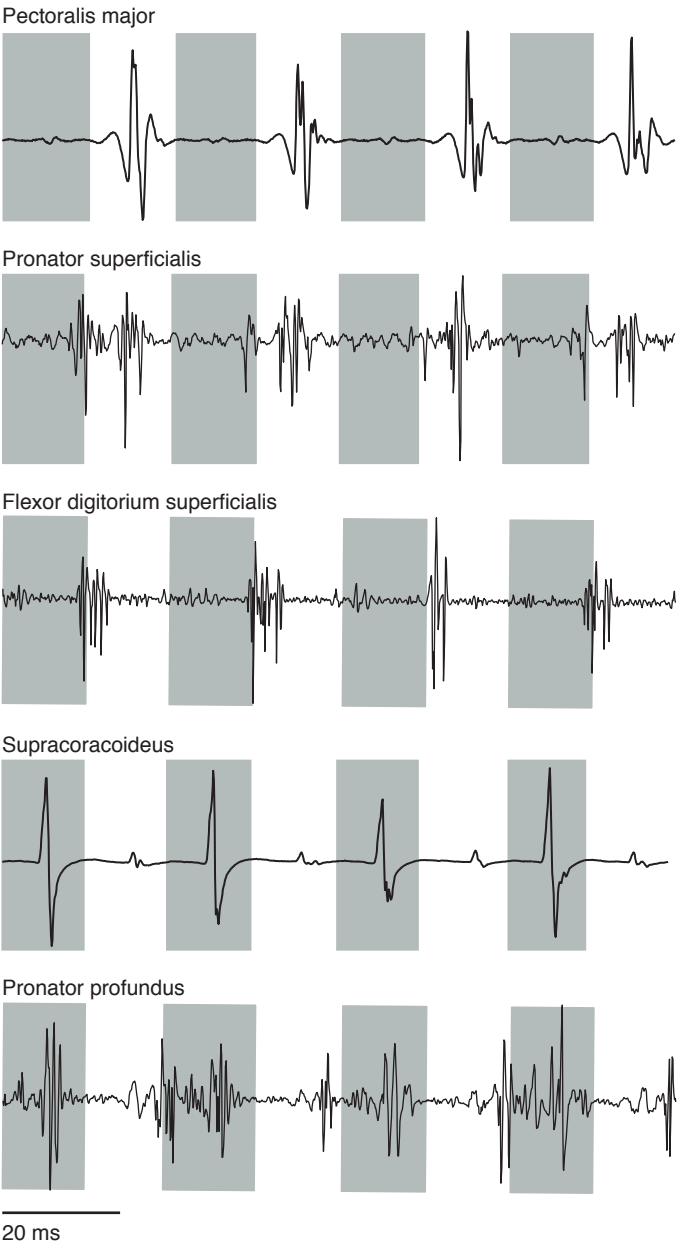


Figure 4

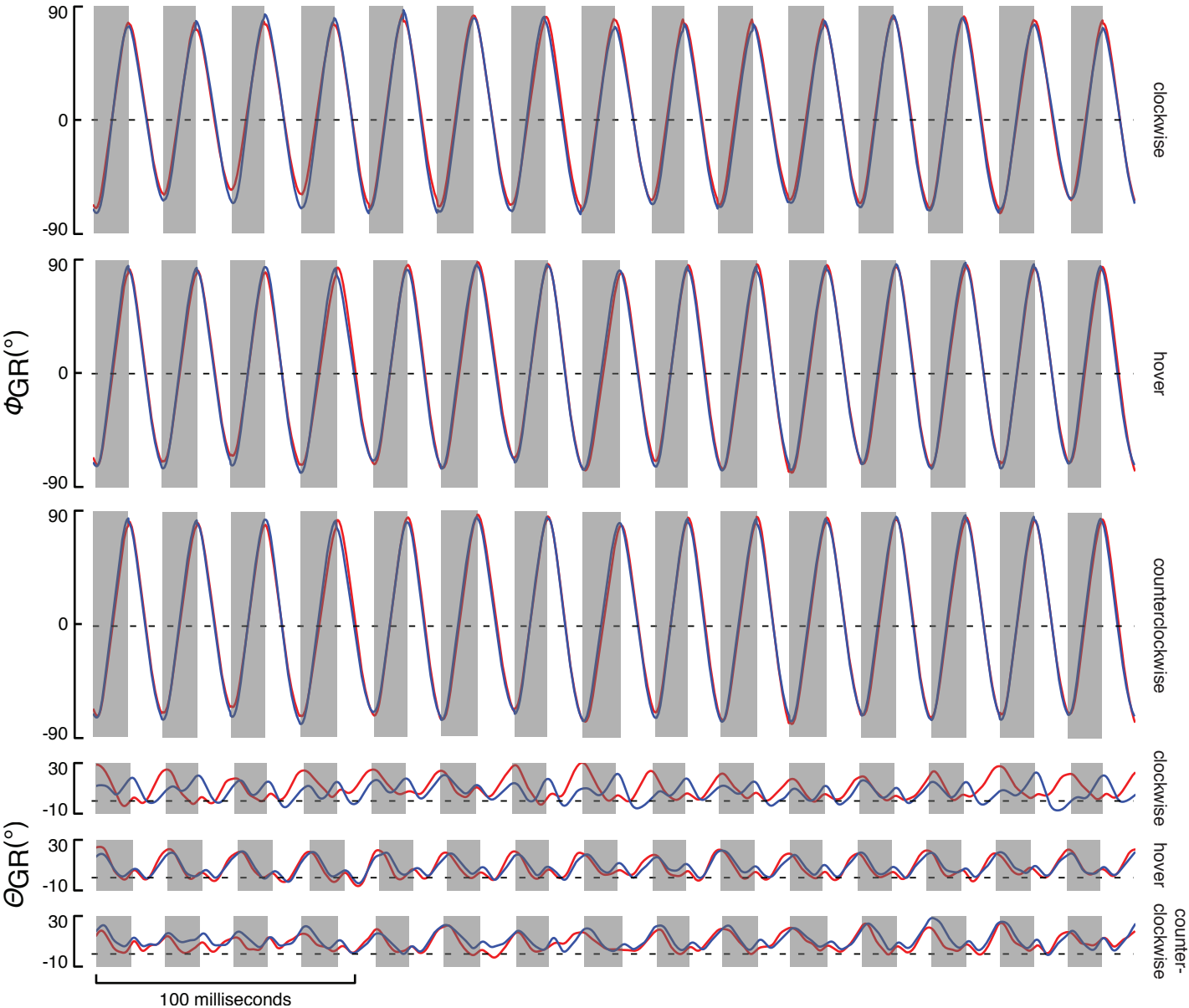


Figure 5

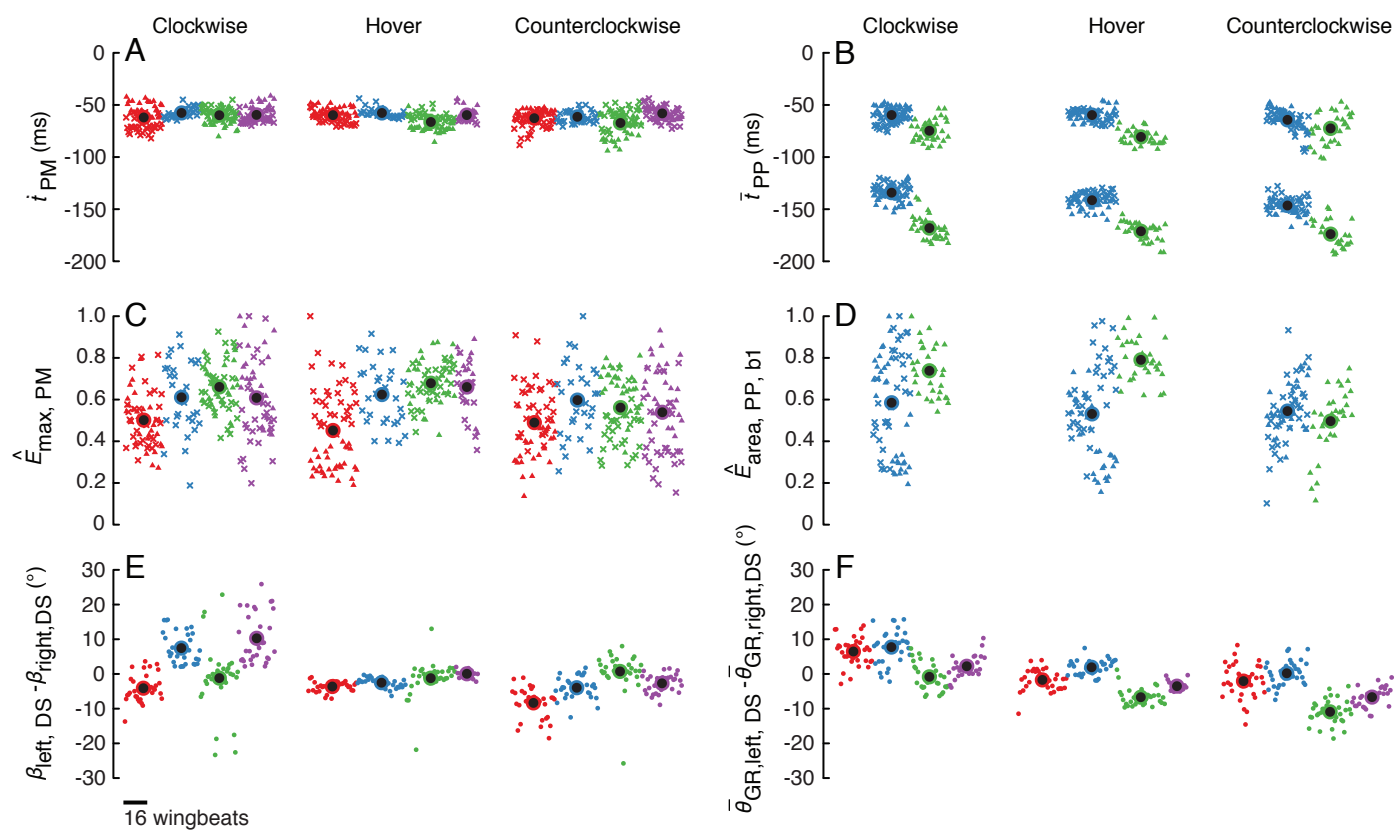


Figure 6

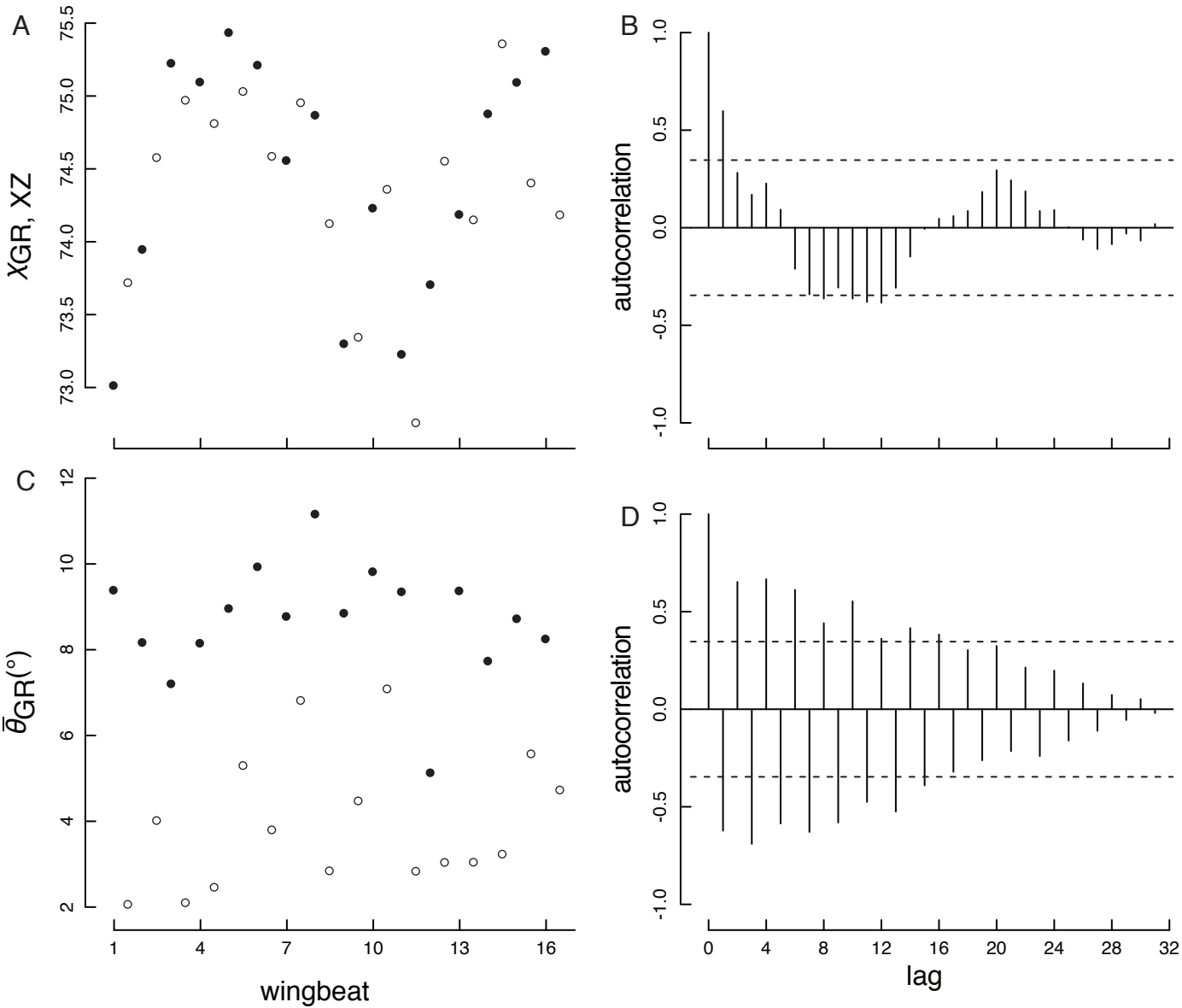
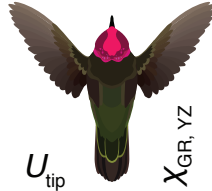


Figure 7



lag	$\chi_{GR, YZ}$	$\chi_{GR, XZ}$	$\theta_{SP}$	$\phi_{SP}$	$\beta$	$\psi$	$U_{tip}$		$\chi_{GR, YZ}$	$\chi_{GR, XZ}$	$\theta_{SP}$	$\phi_{SP}$	$\beta$	$\psi$	$U_{tip}$	lag
-1	0.29	0.18	0.01	0.20	0.17	0.14	0.15	$\bar{\theta}_{GR}$	0.24	0.10	0.01	0.20	0.03	0.20	0.11	-1
-1/2	0.20	0.27	0.03	0.08	0.21	0.22	0.04		0.19	0.22	0.03	0.19	0.04	0.12	0.02	-1/2
0	0.07	0.11	0.00	0.04	0.17	0.26	0.09		0.16	0.10	0.00	0.11	0.00	0.24	0.09	0
1/2	0.04	0.14	0.11	0.04	0.01	0.23	0.20		0.04	0.12	0.06	0.16	0.01	0.15	0.18	1/2
1	0.04	0.10	0.01	0.14	0.19	0.18	0.10		0.17	0.17	0.01	0.24	0.06	0.22	0.09	1
-1		0.13	0.29	0.19	0.29	0.08	0.18	$\chi_{GR, YZ}$		0.13	0.18	0.08	0.25	0.08	0.11	-1
-1/2		0.17	0.25	0.21	0.24	0.16	0.25			0.17	0.19	0.10	0.14	0.16	0.27	-1/2
0		0.09	0.05	0.15	0.16	0.08	0.18			0.09	0.10	0.12	0.11	0.08	0.17	0
1/2		0.04	0.04	0.09	0.07	0.14	0.22			0.04	0.02	0.16	0.13	0.14	0.06	1/2
1		0.07	0.05	0.08	0.10	0.15	0.19			0.07	0.05	0.06	0.19	0.15	0.11	1
-1			0.13	0.12	0.27	0.15	0.16	$\chi_{GR, XZ}$			0.08	0.09	0.15	0.15	0.12	-1
-1/2			0.14	0.14	0.07	0.10	0.25				0.07	0.16	0.04	0.10	0.17	-1/2
0			0.19	0.09	0.11	0.18	0.12				0.14	0.22	0.14	0.18	0.11	0
1/2			0.13	0.18	0.00	0.12	0.28				0.06	0.15	0.02	0.12	0.13	1/2
1			0.08	0.21	0.10	0.21	0.11				0.14	0.22	0.07	0.21	0.10	1
-1				0.16	0.15	0.23	0.11	$\theta_{SP}$				0.20	0.01	0.20	0.01	-1
-1/2				0.13	0.20	0.18	0.04					0.08	0.08	0.18	0.01	-1/2
0				0.17	0.10	0.09	0.04					0.09	0.01	0.22	0.02	0
1/2				0.11	0.13	0.25	0.14					0.18	0.04	0.17	0.03	1/2
1				0.26	0.19	0.15	0.07					0.20	0.01	0.18	0.08	1
-1					0.23	0.21	0.17	$\phi_{SP}$					0.17	0.26	0.20	-1
-1/2					0.22	0.12	0.19						0.19	0.12	0.11	-1/2
0					0.11	0.17	0.00						0.11	0.08	0.00	0
1/2					0.15	0.15	0.03						0.20	0.26	0.08	1/2
1					0.07	0.14	0.26						0.20	0.17	0.19	1
-1						0.19	0.11	$\beta$						0.20	0.07	-1
-1/2						0.13	0.07							0.17	0.08	-1/2
0						0.14	0.04							0.19	0.01	0
1/2						0.19	0.12							0.24	0.10	1/2
1						0.21	0.07							0.23	0.02	1
-1							0.17	$\psi$							0.21	-1
-1/2							0.11								0.24	-1/2
0							0.24								0.11	0
1/2							0.23								0.28	1/2
1							0.33								0.32	1

Figure 8

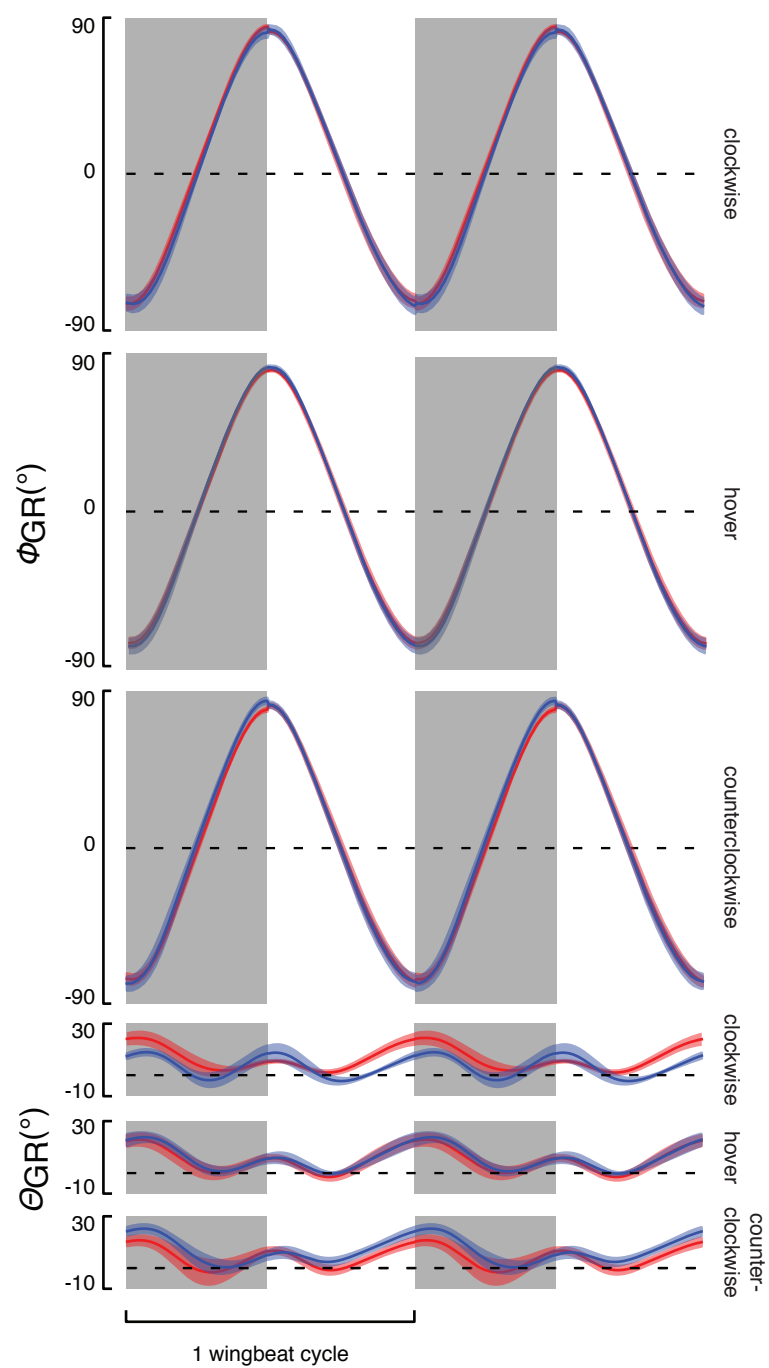


Figure 9

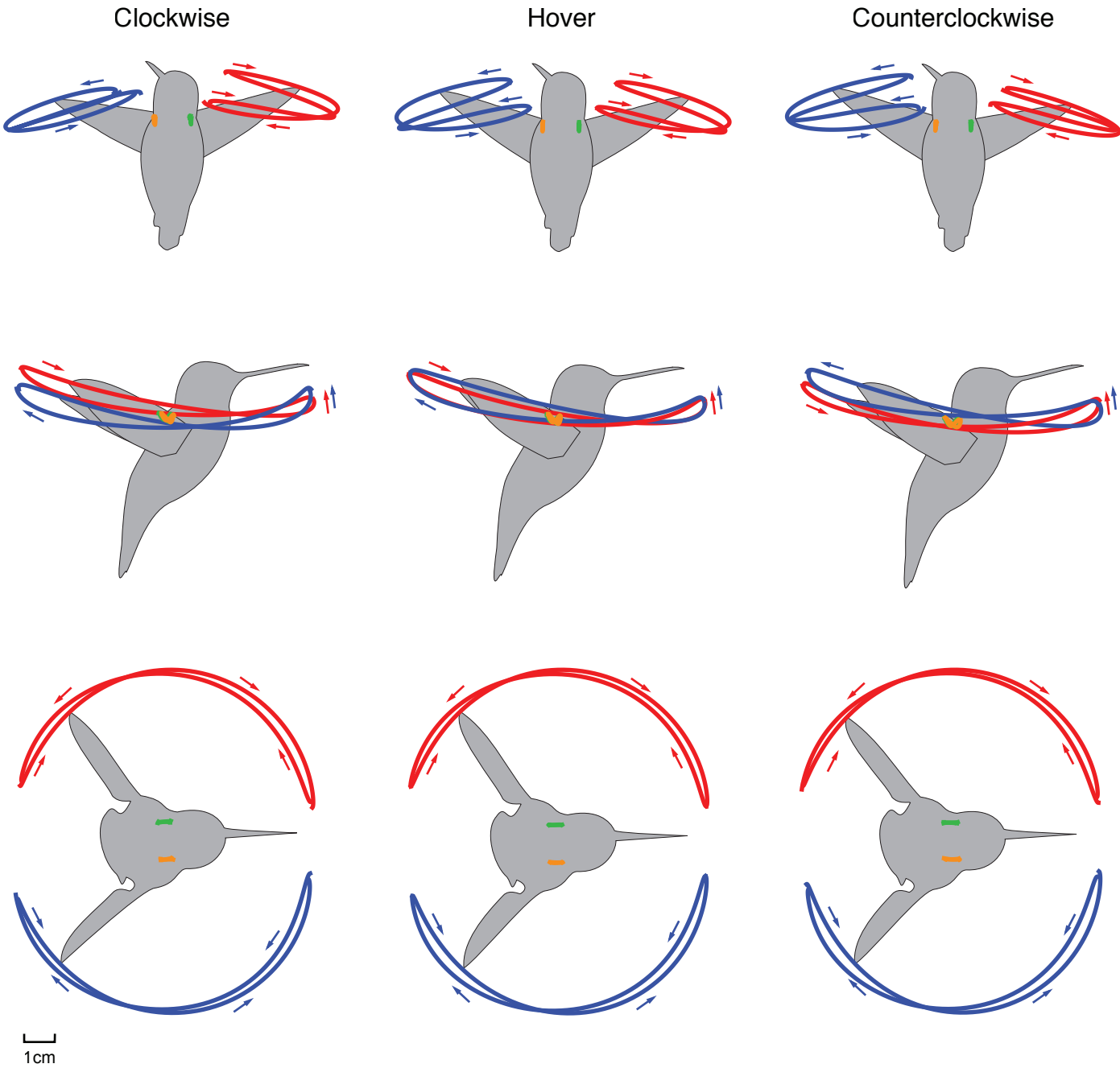
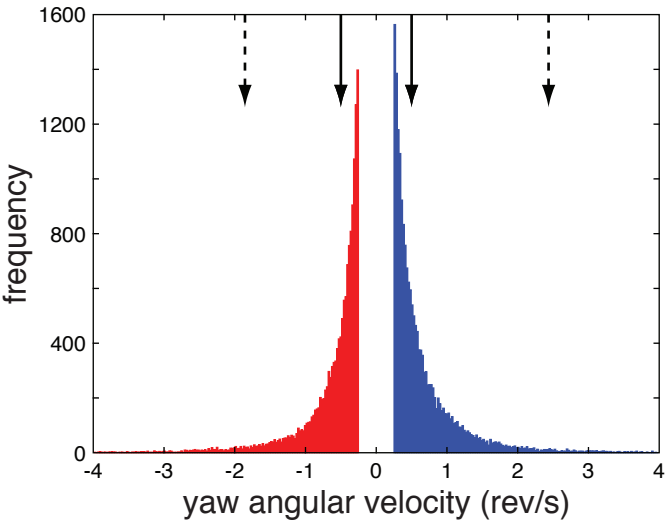




Figure 10



**Table 1.** Variables used to describe the kinematic and electromyographic features of hovering and yaw turns in hummingbirds. Kinematic variables were calculated separately for each down- and up-stroke. Electromyographic variables were calculated over the wingbeat, which included two distinct bursts for the PP and PS muscles.

Variable	Symbol
<i>Electromyographic Features</i>	
normalized maximum spike amplitude	$\hat{E}_{\max}$
normalized rectified area	$\hat{E}_{\text{area}}$
time of the first spike	$\hat{t}$
average spike time	$\bar{t}$
<i>Kinematic Features</i>	
yaw angle	$\psi$
wingtip speed	$U_{\text{tip}}$
body angle, lateral	$\chi_{\text{GR}, \text{XZ}}$
body angle, frontal	$\chi_{\text{GR}, \text{YZ}}$
position angle	$\phi_{\text{GR}}$
elevation angle	$\theta_{\text{GR}}$
average elevation angle	$\bar{\theta}_{\text{GR}}$
stroke plane angle	$\beta$
stroke amplitude	$\Phi_{\text{SP}}$
elevation amplitude	$\Theta_{\text{SP}}$



**Table 2.** Morphological parameters of the four male Anna's hummingbirds (*Calypte anna*) used in the study. Body mass ( $m$ ) is the mean of measurements taken before and after each trial. The wing size parameters, wing length ( $R$ ) and wing area ( $S$ ), as well as the wing shape parameters of aspect ratio ( $AR$ ) and non-dimensional radii of the first ( $\hat{r}_1(S)$ ), second ( $\hat{r}_2(S)$ ), and third ( $\hat{r}_3(S)$ ) moments of wing area were calculated from a digital photograph of a single wing. The wing area and aspect ratio are calculated for two wings to allow for comparisons with other measurements of hovering animals (Ellington, 1984).

Bird	$m$ (g)	Side	$R$ (mm)	$S$ ( $mm^2$ )	$AR$	$\hat{r}_1(S)$	$\hat{r}_2(S)$	$\hat{r}_3(S)$
1	4.20	Left	48.66	1323.70	7.16	0.4332	0.5101	0.5643
		Right	46.25	1098.30	7.79	0.4061	0.4816	0.5368
2	4.21	Left	50.43	1247.30	8.16	0.4117	0.4850	0.5377
		Right	52.68	1389.30	7.99	0.4243	0.4998	0.5535
3	4.06	Left	50.51	1270.40	8.03	0.4241	0.5023	0.5579
		Right	51.18	1378.90	7.60	0.4395	0.5150	0.5692
4	4.64	Left	47.56	1165.20	7.76	0.4258	0.5003	0.5537
		Right	51.26	1402.90	7.49	0.4354	0.5101	0.5636

**Table 3.** Average wingbeat frequencies ( $f$ , Hz) and stroke amplitude differences ( $\Delta\Phi$ , °) for four adult male Anna's hummingbirds (*C. anna*) during hovering and turning. The number of wing strokes ( $n$ ) is provided by bird and treatment. The stroke amplitudes are presented as left minus right differences for the downstroke (DS) and upstroke (US). Statistical analysis of the wingtip speed and stroke amplitude is provided in table 7.

Bird	Clockwise				Hovering				Counterclockwise			
	$n$	$f$	$\Delta\Phi_{DS}$	$\Delta\Phi_{US}$	$n$	$f$	$\Delta\Phi_{DS}$	$\Delta\Phi_{US}$	$n$	$f$	$\Delta\Phi_{DS}$	$\Delta\Phi_{US}$
1	38	41.59	0.00	-8.46	33	40.54	-2.52	-1.61	32	39.88	-15.03	-6.39
2	32	39.49	14.75	6.07	32	39.63	3.32	4.10	44	39.76	2.21	8.75
3	32	39.81	-5.85	-10.85	33	39.69	-12.46	-12.03	33	40.58	-13.91	-6.58
4	31	37.7	6.09	-2.44	30	36.84	-4.44	-4.75	15	36.76	-7.21	-0.33

**Table 4.** The intra-class correlation coefficients (ICC) for the intensity and timing measures of the Pectoralis major, Pronator profundus, and Pronator superficialis muscles during hovering, and clockwise and counter-clockwise yaw turns. The left and right sides were calculated separately for the Pectoralis major and the average values are presented here. Only one side was available for each of the Pronator profundus and Pronator superficialis.

maneuver	intensity	timing
<i>Pectoralis major</i>		
clockwise	0.19	0.52
hovering	0.43	0.51
counter-clockwise	0.41	0.35
<i>Pronator profundus</i>		
clockwise	0.15	0.79
hovering	0.35	0.82
counter-clockwise	0.26	0.49
<i>Pronator superficialis</i>		
clockwise	0.23	0.52
hovering	-0.01	0.74
counter-clockwise	0.40	0.55

**Table 5.** The intra-class correlation coefficients (ICC) for whole body kinematic features, the yaw angle ( $\Psi$ ) and body kinematics (lateral body angle,  $\chi_{GR, XZ}$ , frontal body angle,  $\chi_{GR, YZ}$ ), and for left-right wing kinematics, the wingtip speed ( $U_{tip}$ ), average elevation angle ( $\bar{\theta}_{GR}$ ), stroke plane angle ( $\beta$ ), stroke amplitude ( $\Phi_{SP}$ ), and elevation amplitude ( $\Theta_{SP}$ ). The up- and down-strokes were analyzed separately.

	clockwise	hovering	counter-clockwise
$\Psi_{DS}$	-0.01	-0.01	0.01
$\Psi_{US}$	-0.03	-0.02	-0.02
$\chi_{GR, XZ, DS}$	0.37	0.00	0.08
$\chi_{GR, XZ, US}$	0.34	0.11	0.08
$\chi_{GR, YZ, DS}$	0.60	0.19	0.39
$\chi_{GR, YZ, US}$	0.58	0.17	0.30
$U_{tip, DS}$	0.68	0.78	0.62
$U_{tip, US}$	0.58	0.75	0.55
$\bar{\theta}_{GR, DS}$	0.48	0.70	0.62
$\bar{\theta}_{GR, US}$	0.60	0.59	0.54
$\beta_{DS}$	0.50	0.17	0.45
$\beta_{US}$	0.61	0.53	0.42
$\Phi_{SP, DS}$	0.62	0.61	0.59
$\Phi_{SP, US}$	0.49	0.60	0.48
$\Theta_{SP, DS}$	0.16	0.16	0.17
$\Theta_{SP, US}$	0.30	0.05	0.09



**Table 6.** Mixed model ANOVA of yaw angle ( $\psi$ ) and body kinematics (lateral body angle,  $\chi_{GR, XZ}$ , frontal body angle,  $\chi_{GR, YZ}$ ) by maneuver. Bird was included a random effect within the model. Two post-hoc comparison were made for models with significant ANOVAs: clockwise versus hovering (ck-hv) and counter-clockwise versus hovering (ct-hv).

Variable	d.f.	<i>F</i>	<i>P</i>	<i>P</i> <sub>ck-hv</sub>	<i>P</i> <sub>ct-hv</sub>
$\psi_{DS}$	2,6	225.84	< 0.0001	< 0.0001	< 0.0001
$\psi_{US}$	2,6	521.79	< 0.0001	< 0.0001	< 0.0001
$\chi_{GR, XZ, DS}$	2,6	3.95	0.0804	-	-
$\chi_{GR, XZ, US}$	2,6	4.23	0.0714	-	-
$\chi_{GR, YZ, DS}$	2,6	1.41	0.3143	-	-
$\chi_{GR, YZ, US}$	2,6	1.41	0.3155	-	-

**Table 7.** Mixed model ANOVA of wingbeat kinematics: wingtip speed ( $U_{\text{tip}}$ ), average elevation angle ( $\bar{\theta}_{\text{GR}}$ ), stroke plane angle ( $\beta$ ), stroke amplitude ( $\Phi_{\text{SP}}$ ), and elevation amplitude ( $\Theta_{\text{SP}}$ ). Other details as in table 4.

Variable	d.f.	$F$	$P$	$P_{\text{ck-hv}}$	$P_{\text{ct-hv}}$
$U_{\text{tip, DS}}$	2,6	4.00	0.0786	-	-
$U_{\text{tip, US}}$	2,6	4.8	0.0570	-	-
$\bar{\theta}_{\text{GR, DS}}$	2,6	70.71	< 0.0001	< 0.0001	0.0007
$\bar{\theta}_{\text{GR, US}}$	2,6	10.46	0.0111	0.0074	0.1833
$\beta_{\text{DS}}$	2,6	2.00	0.2155	-	-
$\beta_{\text{US}}$	2,6	6.42	0.0323	0.0384	0.3734
$\Phi_{\text{SP, DS}}$	2,6	17.58	0.0031	0.0005	0.0485
$\Phi_{\text{SP, US}}$	2,6	1.31	0.3383	-	-
$\Theta_{\text{SP, DS}}$	2,6	23.28	0.0015	< 0.0001	0.1100
$\Theta_{\text{SP, US}}$	2,6	11.84	0.0083	0.0008	0.4128